

REF 4739
CONF. 931069-1

EFFECT OF INTERNAL HEATING DURING HOT COMPRESSION TESTING
ON THE STRESS-STRAIN BEHAVIOR
AND HOT WORKING CHARACTERISTICS OF ALLOY 304L

by

M. C. Mataya and V. E. Sackschewsky

RECEIVED
MAY 06 1983
OSTI

ABSTRACT

The temperature change, due to the conversion of mechanical deformation to internal heat, and its effect on the as-measured stress-strain behavior of alloy 304L was investigated by means of initially isothermal (temperature of specimen, compression dies, environment equilibrated at initiation of test) uniaxial compression of laboratory sized cylindrical specimens. Strain rate was varied in the range 0.01 s^{-1} to 1 s^{-1} where the thermal state of the test specimen varied from nearly isothermal to nearly adiabatic, respectively. Specimens were deformed in the temperature range of 750°C to 1150°C to a strain of 1. The change in specimen temperature with applied strain was calculated via finite element analysis from the as-measured stress-strain data and selected predictions were confirmed with embedded thermocouples to verify the model employed. Temperature was found to increase in a near linear manner at the highest strain rate, consistent with the fact that temperature rise is theoretically a linear function of strain for an adiabatic case. As strain rate was lowered, heat transfer from the super heated specimen to the relatively cooler dies caused sample temperature to increase and then decrease with strain as the sample thinned

DISTRIBUTION OF THIS DOCUMENT IS UNLIMITED

for MASTER

and specimen-die contact area increased. As-measured stress was corrected, for softening associated with deformational heating, by linear interpolation of the instantaneous stress-temperature behavior which was found to vary significantly with strain. The resulting isothermal flow curves were compared to those predicted by a simplified method suggested by Thomas and Shrinivasan and the origin of differences are discussed. Strain rate sensitivity, activation energy for deformation, and the peak in the flow curve associated with the onset of dynamic recrystallization were determined from both as-measured and isothermal stress-strain data and found to vary widely. The impact of utilizing as-measured stress-strain data, not corrected for internal heating, on the results of a number of published investigations is discussed.

M.C. MATAYA, Associate Scientist, is with EG&G Rocky Flats, Inc., Golden, CO 80402-0464. V.E. SACKSCHEWSKY, formerly with EG&G Rocky Flats, Inc., is retired.

DISCLAIMER

This report was prepared as an account of work sponsored by an agency of the United States Government. Neither the United States Government nor any agency thereof, nor any of their employees, makes any warranty, express or implied, or assumes any legal liability or responsibility for the accuracy, completeness, or usefulness of any information, apparatus, product, or process disclosed, or represents that its use would not infringe privately owned rights. Reference herein to any specific commercial product, process, or service by trade name, trademark, manufacturer, or otherwise does not necessarily constitute or imply its endorsement, recommendation, or favoring by the United States Government or any agency thereof. The views and opinions of authors expressed herein do not necessarily state or reflect those of the United States Government or any agency thereof.

I. INTRODUCTION

Compression is a particularly useful technique to determine a material's response to plastic deformation at temperatures, strain rates, and to strains typically encountered during conventional hot working processes such as forging. The mechanical response is revealed by the measured stress-strain, σ - ϵ , curve, also referred to as flow curve, while the microstructural response is determined by microscopic examination of the deformed test sample. Flow curves for metals and alloys vary depending on the applied strain rate, $\dot{\epsilon}$, temperature, T , and starting microstructure. They can be used comparatively to obtain information about a materials strain rate sensitivity, m , work hardening rate, n , activation energy for deformation, Q_{DEF} , and equipment loading during forming operations. Flow curves are also useful for identifying the deformation conditions associated with dynamic recrystallization, which causes a sharp reduction in σ with increasing ϵ as recrystallization progresses.

More recently, finite element analysis (FEA) is being widely applied in the computer simulation of plastic deformation during metal forming operations.^[1-8] The reliability of these simulations can be extremely sensitive to the accuracy of the input data provided to the model. This in turn has spawned a need for accurate σ - ϵ characterization. The accuracy of measured σ - ϵ data from compression is typically degraded by friction between sample and die, causing barrelling and nonuniform strain in the sample, and by internal heating of the sample, which

reduces the flow stress of materials that exhibit thermally activated plastic deformation.⁹ Lubrication techniques have been developed to minimize frictional effects. However, as-measured σ - ϵ curves and associated analysis reported in the literature have generally been presented without correction for deformational heating.¹⁰

At high ϵ , the heat generated in a test sample is essentially retained during the short duration of the test and the rise in T can be easily calculated without consideration of heat loss to the environment. Isothermal σ - ϵ curves can be obtained by interpolation of the σ - T data at each increment in ϵ from as-measured σ - ϵ data developed at differing T . Semiatin *et al*⁷ employed this technique to correct as-measured σ - ϵ curves of Ti-6242 for use in finite element simulation of metal flow during forging of a turbine disk. As ϵ is lowered, more time is available for heat transfer during the test and dissipation of the heat from deformation to the environment reduces the temperature increase in the sample. Laasraoui and Jonas^{11,12}, utilizing a similar technique, showed that correction of the as-measured σ - ϵ data for internal heating during hot compression testing provided a significantly more precise determination of the static recrystallization kinetics for various low carbon steels.

At a sufficiently low value of ϵ , the heat is dissipated, as it is generated, to the surrounding environment and the test progresses isothermally. Thus, in the two ϵ extremes, the bounds

of which are determined by test sample geometry and other test conditions which govern heat transfer to the environment, isothermal behaviors can be obtained rather easily. However, in the intermediate $\dot{\epsilon}$ realm, the process is neither adiabatic nor isothermal. Sample temperature can be measured via embedded thermocouples, but testing is complex and costly and embedded thermocouples perturb the σ - ϵ response of the specimens. Therefore, methods to calculate temperature rise in this intermediate $\dot{\epsilon}$ realm would be very useful.

Thomas and Shrinivasan¹³, based on the compression data of Charpentier *et al.*,¹⁴ have recently proposed a simple empirical approximation to determine the isothermal flow curves in this intermediate $\dot{\epsilon}$ realm to facilitate the calculation of isothermal flow curves. Their method, which assumes the achievement of a steady state stress at relatively low strain, e.g. 0.2, appears to provide an appropriate σ correction for materials with high stacking fault energy, SFE, e.g. aluminum, which undergo rapid dynamic recovery and exhibit little work hardening. However, it may not be effective for materials with low SFE, e.g. 304L, which typically undergo limited dynamic recovery and exhibit either work hardening or softening due to dynamic recrystallization beyond a $\dot{\epsilon}$ of 0.2.^{15,16}

The purpose of this investigation was to obtain accurate isothermal σ - ϵ data for alloy 304L in the $\dot{\epsilon}$ realm where the thermal state of the test specimen is neither isothermal nor adiabatic. Deformational heating of test specimens was studied

by performing a thermal-mechanically coupled finite-element-analysis of the compression test. The calculated instantaneous σ - ϵ - T behavior was used to determine the isothermal flow curves. The results are compared to those obtained by the method of Thomas and Shrinivasan. Both as-measured and isothermal sets of σ - ϵ data were utilized to calculate strain rate sensitivity, m , strain to initiate dynamic recrystallization, ϵ_p , and activation energy for deformation, Q_{DEF} . The results from each set are compared.

II. EXPERIMENTAL PROCEDURE

A. Material

The chemical composition of the 304L alloy used in this investigation is given in Table I. The alloy was arc-melted in air and then argon-oxygen decarburized prior to casting a 356-mm-diameter electrode. The electrode was vacuum-arc-remelted into a 406-mm-diameter ingot. The ingot was bloomed to a 127-mm round-cornered-square bar on a continuous mill at 1150°C and hot rolled to a 38.1-mm-diameter bar. Rolling started at 1100°C and finished at approximately 900°C. The bar was swaged at room temperature to a 15.2-mm-diameter rod. The rod was solution heat treated at 1000°C for 30 minutes and water quenched providing the starting material for the investigation. Prior studies of this particular heat of 304L showed that this heat treatment provides a well annealed, relatively dislocation free matrix with equiaxed grains having an average grain diameter of 0.038- μm .¹⁵

B. Elevated Temperature Compression Testing

The test setup is shown schematically in Fig. 1. Compression testing was accomplished in a 250 KN servo-hydraulic testing machine (manufactured by M.T.S. Corp.) outfitted with an electric resistance clam-shell furnace. The vertical load column was composed of two opposing Astroloy rams, which were hollowed to facilitate heating, and flat smooth (lapped to 8 RMS surface finish with opposite faces parallel to within 0.0127-mm over a 69.85-mm diameter) SiN compression dies, fitted to the end of the rams. Cylindrical compression samples, 12.7-mm-diameter by 19.05-mm-high, were machined from the heat treated 15.1-mm-diameter rod, with specimen axis parallel to rod axis. The end faces were recessed to form a lubricant well, an effective technique for constraining lubricant to the sliding face during compression.¹⁷ Weis¹⁸ verified the effectiveness of this technique compared to others and determined an optimum well geometry for the specimen used in this investigation, Fig. 1. Various glass lubricants were employed to accommodate the wide range of testing temperatures: Delta Glazes #13 for 750°C, #93 for 850°C, #349M for 950°C, and #347M for 1050°C and 1150°C (products of Atcheson Chemical Co.)

Test specimens were loaded onto the bottom die in the furnace in air, held for 10 min. in the furnace at temperatures between 750°C and 1150°C (specimens required approx. 5 minutes to equilibrate), compressed uniaxially to a strain of 1, and quenched in water immediately after deformation. The time to

quench was between one and two seconds. The velocity of the moving die was varied via computer control in order to apply deformation at a constant $\dot{\epsilon}$ rate of 0.01 s^{-1} , 0.1 s^{-1} , or 1 s^{-1} . Compliance in the load train resulted in deviations in ϵ and $\dot{\epsilon}$ up to about -5 pct with the maximum occurring at the lowest temperature, at which the greatest loads were encountered. Compliance was characterized and appropriate corrections were applied to the measured displacement of the sample obtained from a linear-variable-differential-transformer mounted at the lower end of the moving ram. Values for true σ and true plastic ϵ (hereafter referred to simply as σ and ϵ) were calculated, with conventional methods, from the as-measured load and corrected displacement data. The strain was assumed uniform throughout the sample. Calculated and as-measured values of final ϵ were typically within 1 to 2 pct.

Heating of test samples during compressive deformation was measured via embedded thermocouples located at three different positions in the test sample: at the specimen axis and near the specimen-die interface (1.3-mm from the specimen face), at the specimen center (mid-height, mid-diameter), and at the mid-height, outer-diameter position. Millivolt signals from the thermocouples were recorded simultaneously at 0.001 s intervals.

C. Determination of Isothermal Stress vs. Strain Behavior

C.1. A method suggested by Thomas and Shrinivasan

The as-measured σ - ϵ data were corrected for deformational heating via two different techniques. The first, proposed by

Thomas and Shrinivasan¹³, hereafter referred to as the T&S method, consists first of calculating the change in sample temperature, ΔT , with applied ϵ by the following conventional formulation:

$$\Delta T = (\eta / \rho C_p) \int_0^{\epsilon_f} \sigma \, d\epsilon \quad [1]$$

where ρ is density, C_p is heat capacity per unit mass, ϵ_f is the final true plastic strain, and η is the fraction of deformational energy which appears as a temperature rise. For adiabatic conditions, η is usually assumed to be 0.95. Second, a single σ - T relationship is constructed from the as-measured σ - ϵ data at different T . The relationship is generated at a single, low value of ϵ where deformational heating is assumed minimal. Third, the as-measured σ is corrected at a given value of ϵ based on the calculated ΔT and corresponding $\Delta\sigma$ calculated from the σ - T relationship.

Based on the experimental results of Charpentier et al¹⁴, who measured ΔT in aluminum alloy 2024 compression samples after an applied ϵ of 0.7, Thomas and Shrinivasan suggest that η varies linearly with the logarithm of $\dot{\epsilon}$, equalling 0 at 0.001 s⁻¹ or less and 0.95 at 1.0 s⁻¹ or greater. Following their suggestion, the value of η is expressed as follows,

$$\eta = 0.316 \log_{10} \dot{\epsilon} + 0.95 \quad [2]$$

In this study, ΔT was calculated, via equations 1 and 2, for each measured increment of ϵ , approximately 0.005. The trapezoid

rule was used for the integration in equation 1. For each ϵ , a single σ -T relationship was constructed from the as-measured σ - ϵ data for various T and at a ϵ of 0.2. The σ -T data was statistically fit with a cubic polynomial which was used to calculate the increment of stress softening associated with ΔT at each value of ϵ . This increment was then added to the as-measured value of σ to approximate the value of σ that would be obtained if the test was conducted isothermally.

C.2. A method employing finite element analysis

A second method for calculating isothermal flow curves from as-measured σ - ϵ data was developed in this study. It utilizes finite-element-analysis (FEA) to calculate the instantaneous T in the compression sample with increasing ϵ . This is a refinement to the T&S method in that geometric effects on the heat transfer to the dies as the specimen is compressed is included in the temperature calculations. Also, this method does not implicitly assume that flow stress is constant with increasing ϵ nor that the flow curve shape is constant for varying T as is the case in the T&S method. The isothermal response of σ to ϵ is calculated from the resulting instantaneous σ -T relationships, determined at each 0.01 increment of ϵ .

Figure 1 shows a schematic of the finite element model used to simulate the compression tests. The MARC finite element code (copyright of MARC Analysis Research Corp., Inc., Palo Alto, CA) was used for the simulation. The analysis was thermal-mechanically coupled so that σ , ϵ and T were calculated for each

time increment during the simulation. The analysis assumes symmetry about the center axis, oriented in the vertical direction in Fig. 1 and in the test setup, and about a perpendicular plane through the mid-height of the cylinder. Axial symmetry implies that the system can be represented by a two-dimensional model. Vertical symmetry implies that only one-half of the cylinder must actually be modeled. Thus, the model shown in Figure 1 represents one quadrant of a vertical cross section through the cylinder. The quadrant of the 12.7-mm diameter by 19.05-mm high (0.5 in x 0.75 in) cylinder is represented by a mesh of 20 four-node quadrilateral elements in the radial direction and 16 elements for the half-height. The conversion of mechanical energy to heat was assumed to have an efficiency of 0.95.

The upper die of the compression test setup is represented by the upper rigid die in Fig. 1. Simulated movement of this die was controlled via a subroutine within the code to provide a specified constant true strain rate. A friction coefficient of zero was used between the die and cylinder, based on the observed lack of barrelling on the free surface of compressed samples. Heat transfer via conduction is included between the cylinder and die, and includes a constant film coefficient, independent of σ , ϵ , $\dot{\epsilon}$, and T , for the interface. For this analysis, T of the moving rigid die was assumed to be constant. Radiation from the wall of the cylinder was not included in the model because one would expect radiative heat transfer to be insignificant compared

to conduction for the test environment and geometry encountered in this case, and to include it would dramatically increase the complexity of the analysis. The lower rigid die shown in the model is an imaginary die through the specimen mid-plane, Fig. 1, and its function in the model will be discussed.

Separate FEA analyses were run to simulate each combination of T and ϵ employed experimentally. For each case, the corresponding as-measured σ - ϵ data was used as the specimen flow stress behavior for FEA and the T profile within the specimen was calculated (analogous to equation 1). By extracting the σ , ϵ and T data from the analysis, isothermal σ - ϵ curves can be obtained by linear interpolation.

While in principle the generation of the isothermal curves is straight forward, problems were encountered in the analysis which forced certain approximations. Initial FEA analyses showed a nonuniform distribution of σ and ϵ within the deformed cylinder due to nonuniform T within the cylinder (because of heat transfer at the cylinder-die interface) and the use of T dependent material properties in the model. Thus, the σ - ϵ - T data could not be simply extracted from any one FEA element in the cylinder as would be the case for a uniform distribution. Rather, it was necessary to reduce the multi-valued σ - ϵ - T data obtained from the FEA analysis to single valued data corresponding to that obtained experimentally.

The lower, stationary rigid die shown in the model was introduced to provide an independent calculation of σ . An

average measure of the σ in the cylinder was obtained by dividing the load on the lower rigid die (a standard quantity calculated by the program) by the area at mid-height, obtained by tracking the position of the outer node on this plane. This quantity is analogous to the experimentally measured σ . For the lower die, the friction was also assumed to be zero because nodes on this plane are not subjected to external constraints. However, a film coefficient of zero was used to prevent heat flow from the cylinder to this die, because by symmetry, there is no heat flow in the vertical direction across the mid-plane.

Values of ϵ and T corresponding to the σ values described above were extracted from the FEA results as follows. Strain was taken as the average of the minimum and maximum equivalent plastic ϵ calculated in the cylinder. Typically these two extremes were within 1 to 2 pct. of each other. The calculated T was essentially constant in the radial direction. Temperature at the outer mid-plane node was used for T . This location is consistent with the region used in the calculations for σ . The σ - ϵ - T values were determined at 0.01 increments of ϵ by linear interpolation. Isothermal σ - ϵ curves were then calculated from the resulting five sets of σ - T curves, corresponding to the five starting temperatures, by linear interpolation at each of the 0.01 increments of ϵ .

Values of elastic modulus, thermal expansion coefficient, thermal conductivity, and specific heat as they vary with T , used in the FEA model, are listed in Table II. The coefficient of

heat transfer between specimen and die was determined by matching predicted variations in T with $\dot{\epsilon}$ obtained with FEA, for various arbitrary values of the heat transfer coefficient, to a measured variation (via embedded thermocouple) obtained at 950°C and a $\dot{\epsilon}$ of 0.1 s^{-1} . Preliminary FEA analyses, not shown here, revealed that the temperature profile was most sensitive to the film coefficient for this particular combination of deformation parameters. Figure 2 shows both predicted and as-measured variations of T with $\dot{\epsilon}$. Based on this figure the coefficient was assumed to be $6.54 \times 10^3 \text{ J/sec/m}^2/^{\circ}\text{K}$ (curve C). The slight difference between the as-measured and calculated T at high $\dot{\epsilon}$ may be attributed to the FEA assumption that T of the moving rigid die is constant, equalling that at test initiation. In reality, some of the heat of deformation will be conducted from the specimen to the dies as the test proceeds and, as a result, less heat will be transferred to the warmer dies than predicted by this FEA model. Thus, the real sample T should lie slightly above the predicted T at high $\dot{\epsilon}$, as observed in Fig. 2.

III. RESULTS

A. Calculated Temperature Rise

Figures 3, 4, and 5 show the calculated ΔT with applied $\dot{\epsilon}$ for compression samples deformed at a $\dot{\epsilon}$ of 1 s^{-1} , 0.1 s^{-1} , and 0.01 s^{-1} , respectively. Both predictions, T&S (dashed curves) and FEA (solid curves), are shown. In general, ΔT increases as T decreases because, in equation 1, σ varies inversely with T . For example, Figure 3 shows ΔT is approximately 80°C and 20°C for the

750°C and 1150°C tests conducted at a $\dot{\epsilon}$ of 1 s⁻¹. In this figure, the FEA curves lie slightly below the T&S curves because FEA accounts for heat conduction to the SiN dies, whereas, at this $\dot{\epsilon}$ the T&S analysis assumes η equal to its maximum value, 0.95, which defines the thermal state of the compression sample to be purely adiabatic.

Figures 4 and 5 show that the specimen T predicted by FEA rises rapidly, compared to the T&S prediction, with initial $\dot{\epsilon}$ and then decreases with additional $\dot{\epsilon}$. The drop in ΔT is attributed to the changing sample geometry as the test progresses. The reduction in sample height (or thickness) decreases the distance from the center of the sample to the die face. This, in turn, increases the T gradient and thus the heat flux. Secondly, the sample increases in diameter. The contact area between the specimen and die increases causing an increase in heat flow as deformation proceeds. Methods which ignore heat transfer and rely only on equation 1 for ΔT can only predict a monotonic increase in temperature, as shown in the figures.

At low $\dot{\epsilon}$ the magnitude of ΔT from FEA is greater than from T&S. In the former, T is calculated from the dynamics of heat generation and flow. In the latter, the increase in ΔT with $\dot{\epsilon}$ from equation 1 is moderated only by η , which is assumed not to vary with $\dot{\epsilon}$ (actually, it does). Because η was approximated by T&S from measurements at high $\dot{\epsilon}$, e.g. 0.7, η represents an average behavior, underestimating heat retention at low $\dot{\epsilon}$ and overestimating it at high $\dot{\epsilon}$.

Figure 6 shows the measured ΔT with ϵ , acquired from thermocouples embedded in test specimens, compared to corresponding predicted curves. The FEA curves closely approximate the measured behavior, giving validity to the FEA model. Generally, the T&S predictions over estimate the increase in ΔT and do not show the moderation of ΔT with increasing ϵ that occurs because of heat transfer to the compression dies.

B. Stress Versus Temperature

In the T&S scheme, the magnitude of the σ correction depends on the calculated ΔT , equation 1, in the test sample, and on the σ -T behavior, determined from the measured data at a single low value of ϵ . Figure 7 shows the variation in stress with the initial test T, for strains of 0.2, 0.3, and 0.8, and a $\dot{\epsilon}$ of 1 s^{-1} , obtained from the as-measured σ - ϵ data in Fig. 8. The data for a ϵ of 0.2 was fitted to a cubic polynomial and used in the T&S scheme. For example, Figure 7 shows that for an initial deformation T of 750°C , a ΔT of 100°C results in a stress correction of approximately +40 MPa from the 0.2 ϵ curve.

The three isostrain σ -T curves in Fig. 7 have significantly different slopes, especially at T below 1050°C . Thus, each would yield different σ correction values. For example, the 0.8 ϵ curve gives a stress correction of approx. +75 MPa for a 100°C temperature rise, a value nearly double the one obtained from the 0.2 ϵ curve. The assumption that the 0.2 ϵ curve represents the σ -T behavior for 304L at all ϵ levels appears to be inappropriate due to the relatively low SFE of this alloy and the associated

work hardening which occurs during deformation at high ϵ and low T and dynamic recrystallization at low ϵ and high T. These two phenomena couple to prevent the σ from reaching a steady state stress. Thus, an inherent error in the magnitude of the σ correction is found in the T&S scheme for those materials where the single σ -T relationship developed at low ϵ is not representative of the behavior at high ϵ .

Although not plotted in Figure 7, compression data at temperatures below 750°C show that the difference in the slopes of the three isostrain curves, from 0.2 to 0.8, continues to increase. Thus, for 304L deformed at T below 750°C, the magnitude of error in the calculated σ correction, introduced by employing a single σ -T relationship obtained at a low value of ϵ , would be greater than encountered in this study. As ϵ decreases, the σ -T behaviors for the three ϵ levels approach each other (figures not shown) and the error associated with the ϵ sensitivity of the T&S scheme is reduced.

In the alternative method for σ correction investigated here, the instantaneous T of the test sample is calculated by FEA and a σ -T data set is generated for each 0.01 increment of ϵ . Each is used at its corresponding ϵ to determine, by linear interpolation, the value of σ corresponding to the initial test T.

C. Stress-Strain Behavior: As-measured and Isothermal

Figures 8, 9, and 10 show the σ - ϵ curves for temperatures between 750°C and 1150°C and strain rates of 1 s⁻¹, 0.1 s⁻¹, and

0.01 s⁻¹, respectively. The as-measured and two predicted isothermal behaviors, T&S and FEA, are provided. In each case the as-measured curves lie below the predicted isothermal curves because of the flow softening associated with deformational heating in the test sample. At high $\dot{\epsilon}$ and ϵ , the FEA flow curves lie well above the T&S curves, Fig. 8. In lieu of the similarity of the predicted ΔT , Fig. 3, the discrepancy must result from differences in the correction schemes of the two methods. The low slope of the σ -T curve for a $\dot{\epsilon}$ of 0.2 compared to the 0.8 curve in Fig. 7, the latter being more representative of the σ -T behavior at high $\dot{\epsilon}$, results in a relative insensitivity of σ with T and an undervalued correction to the flow curve by the T&S method.

Figure 9 shows that at a $\dot{\epsilon}$ of 0.1 s⁻¹ the curves derived from the two correction methods are similar with the FEA curve generally giving slightly higher σ values at low $\dot{\epsilon}$ and lower values at high $\dot{\epsilon}$, consistent with the relative change in T calculated by the two methods, Fig. 4. Fig. 10 shows that at the lowest $\dot{\epsilon}$, 0.01 s⁻¹, the FEA curves lie below the T&S curves for lower T, consistent with the overall lower ΔT calculated by FEA and smaller resulting σ correction.

From these figures, the FEA method generally predicts less ΔT in the compression sample as $\dot{\epsilon}$ increases and ϵ decreases (by a factor of about 5 at the highest $\dot{\epsilon}$ and lowest $\dot{\epsilon}$ studied) compared to T&S. The relative position of the flow curves corrected for ΔT by the two methods in Figs. 8, 9, and 10, are explained by the

variation and magnitude of ΔT shown in Figs. 3, 4, and 5. The close correspondence between the as-measured and FEA values of ΔT demonstrates that the FEA flow curves closely represent the true state of the isothermal behavior of alloy 304L. This provides the basis for the following analysis which compares the values of hot working parameters m , Q_{DEF} , and ϵ_p calculated from the as-measured and FEA isothermal σ - ϵ sets of data, Tables III, IV, and V (corresponding to Figs 8, 9, and 10).

D. Heat Retention Efficiency

The heat retention efficiency, η , is assumed by Thomas and Shrinivasan to vary linearly with ϵ , in the realm tested here, as shown by the dashed line in Fig. 11. For comparison, η was calculated from the FEA data (Figs. 3, 4, and 5) by dividing the calculated ΔT by the maximum ΔT for an adiabatic case, the latter value obtained from equation 1 and the as-measured σ - ϵ data. The variation of FEA η is shown in Fig. 11 for two values of ϵ , 0.2 and 0.7. Based on the experimental data on aluminum¹⁴, which is similar to the FEA 304L data, the curves for 304L FEA η were forced through zero at 0.001 s^{-1} and 0.95 at 10 s^{-1} . The FEA data for 304L, which exhibits much less scatter than the aluminum data, demonstrates that the variation of η with $\log \epsilon$ is distinctly nonlinear. Thus, the linear approximation of T&S results in significantly underestimated values of η for 0.2ϵ in the ϵ range from 0.01 s^{-1} to 0.5 s^{-1} and overestimated values for 0.7ϵ from 0.005 s^{-1} to 0.1 s^{-1} . The decrease in η from 0.2 to 0.7ϵ , observed in Fig. 11, is due to changes in sample geometry,

reducing thickness and increasing diameter, with increasing ϵ . Both enhance heat flow from the specimen to the dies and, as a result, the heat retention efficiency, η , is reduced with increasing ϵ . The effect of underestimation of η at low ϵ and overestimation at high ϵ in this ϵ range is that the T&S calculated ΔT for the specimen is likewise under and overestimated compared to the FEA values, as observed in Figs. 4 and 5. Because calculated ΔT is utilized to correct the as-measured stress for deformational heating, similar behaviors can be seen in the σ - ϵ curves, Figs. 9 and 10. At higher $\dot{\epsilon}$, 1 s^{-1} , values of η from the two methods are nearly equal and small differences are observed in ΔT , Fig. 4. The observed differences in the T&S and FEA σ - ϵ curves for this $\dot{\epsilon}$, Fig. 3, are not due to differences in η but instead are due to differences in the application of σ - T - ϵ relationships in calculation of the isothermal σ - ϵ behavior after ΔT is calculated. That is, ϵ is taken at a single low value in the T&S method but is varied in the FEA method. The applicability of the latter technique is demonstrated in Fig. 7 where the σ - T behavior is shown to be highly dependent on ϵ .

E. Strain Rate Sensitivity, m

Strain rate sensitivity, m , is calculated conventionally as follows,

$$m = \Delta \ln \dot{\epsilon} / \Delta \ln \sigma \quad [3]$$

Figure 11 shows the variation of m with T for a $\dot{\epsilon}$ of 0.6. In general, both M(L) and M(H), m in the low (0.01 s^{-1} to 0.1 s^{-1})

and high (0.1 s^{-1} to 1 s^{-1}) $\dot{\epsilon}$ regimes, respectively, increase to a value of about 0.2 as T rises indicating the increased importance of time dependent thermally activated flow at higher temperatures. $M(L)$ is greater over most of the T range studied. This indicates that thermally activated plastic flow, which relieves internal stress through dislocation climb and recovery processes, is allowed to a greater extent by the additional time for deformation associated with the lower $\dot{\epsilon}$ regime.

The values of $M(L)$ and $M(H)$ calculated from the isothermal σ - ϵ data (solid curves in Fig. 11), hereafter referred to as isothermal $M(L)$ and $M(H)$, are greater than the corresponding values calculated from the as-measured data (dashed curves) over the T range studied. This difference is greater in the lower $\dot{\epsilon}$ regime indicating that the usage of m , derived from anisothermal test data, to estimate the change in flow stress due to a change in $\dot{\epsilon}$ will result in a significant under estimation of the change in flow stress.

Figure 13 shows the variation of m with $\dot{\epsilon}$ at a T of 950°C . At low $\dot{\epsilon}$, the values for isothermal $M(L)$ and $M(H)$ are nearly equal to their corresponding as-measured values due to the relatively small amount of deformational heating that occurs at low $\dot{\epsilon}$ (Figs. 4, 5, and 6). As $\dot{\epsilon}$ increases, m is significantly under estimated from the anisothermal data. Similar to the variation of m with T in Figure 11, the under estimation is greater in the lower $\dot{\epsilon}$ regime. The strong increase in isothermal m with $\dot{\epsilon}$ is probably associated with an increased dislocation

density and an associated increase in the driving force for dislocation rearrangement and annihilation. The strong upturn in $M(L)$ at a strain of 0.4 corresponds to softening in the σ - ϵ curve at a $\dot{\epsilon}$ of 0.01 s^{-1} at 950°C , Fig. 10. Such softening is generally associated with the onset of dynamic recrystallization and has been demonstrated in this alloy.¹⁵ The onset of dynamic recrystallization has been shown to be $\dot{\epsilon}$ dependent, with an increase in $\dot{\epsilon}$ causing an increase in the critical level of ϵ for dynamic recrystallization. This ϵ is approximately equal to that value associated with the initial peak in the flow curve, ϵ_p . The value of ϵ_p for a $\dot{\epsilon}$ of 0.01 s^{-1} , Fig. 10, compared to that for 0.1 s^{-1} , Fig. 9, increases from 0.4 to 0.6. The continued hardening of the 0.1 s^{-1} data coupled with the softening of the 0.01 s^{-1} data in this ϵ range causes the sharp increase in $M(L)$ between 0.4 and 0.6 ϵ observed in Fig. 13. At high strains, $\epsilon > 0.8$, $M(L)$ reaches a constant value due to the progression of dynamic recrystallization and the attainment of a steady state stress level at both strain rates, 0.01 s^{-1} and 0.1 s^{-1} .

F. Activation Energy for Deformation, Q_{DEF}

The activation energy for deformation, Q_{DEF} , appears in the equation attributed to Zener-Hollomon,¹⁹

$$Z = \dot{\epsilon} \exp(Q_{DEF}/RT) \quad [4]$$

where T is the absolute temperature (in kelvin), R is the universal gas constant, and Z is the Zener-Hollomon parameter. Zener and Hollomon suggest that flow stress is a function of Z and ϵ . For the calculation of Q_{DEF} , the following general

expression for σ is assumed:

$$\sigma = f(\dot{\epsilon}) Z^u \quad [5]$$

where $f(\dot{\epsilon})$ is some function of $\dot{\epsilon}$ and u is a constant. The value of Q_{DEF} was calculated as a function of $\dot{\epsilon}$ and T , for applied strains of 0.2 and 0.6, from both the as-measured and isothermal σ - $\dot{\epsilon}$ curves. Figures 14 and 15 show the variation in σ , after an applied $\dot{\epsilon}$ of either 0.2 or 0.6, respectively, with inverse T for the three strain rates studied. Each set of data was fitted to a cubic polynomial and values of inverse T at constant σ were calculated for each $\dot{\epsilon}$.

Figures 16 and 17 show the variation of $\ln \dot{\epsilon}$ with inverse T for different σ levels. The slope of each curve corresponds to Q_{DEF}/R , from equation 4. It has been general practice in the literature to calculate Q_{DEF} in the hot working range from as-measured σ - $\dot{\epsilon}$ data. The data in graphs similar to Figs. 16 and 17 generally exhibit a nearly linear behavior and thus Q_{DEF} is often assumed to be constant over the $\dot{\epsilon}$ range studied. In fact, examination of the as-measured σ - $\dot{\epsilon}$ data in Figs. 16 and 17 could lead to the same conclusion. The assumption of constant Q_{DEF} , independent of T , $\dot{\epsilon}$, ϵ , is an attractive assumption because it greatly simplifies subsequent utilization of Z in constitutive relationships. However, the isothermal data in the figures exhibits a distinct curvature which shows that Q_{DEF} decreases with decreasing $\dot{\epsilon}$. This behavior is consistent with the fact that Q_{DEF} in the creep realm is lower than Q_{DEF} in the hot working realm. Evidence for a continuous variation of Q_{DEF} is apparent here.

The data sets in Figures 16 and 17 were fitted with a 2nd order polynomial and Q_{DEF} was calculated by differentiating the polynomial for the various deformation conditions, Table VI. This assumption introduces some error in the calculated values for Q_{DEF} at the highest and lowest ϵ , but without expanding the range of ϵ studied, the variation of Q_{DEF} outside this range is undefined, limiting curve fitting to a data set of three points. At low ϵ , 0.2, values for Q_{DEF} from the as-measured and isothermal data are similar because of the limited amount of sample heating at low ϵ . The average Q_{DEF} obtained from the two sets of data is 417 and 413 kJ/mole, respectively. At a ϵ of 0.6, however, values of Q_{DEF} from as-measured and isothermal data are significantly different. Average values for Q_{DEF} are 407 and 356 kJ/mole, respectively. In this case, significant heating of the sample occurs as a result of the greater applied ϵ . Samples deformed at the high ϵ retain most of the deformational heat causing significant rise in T and decrease in σ as deformation proceeds. Comparing the behavior of the as-measured data to the isothermal data at constant σ , Figs. 14 and 15, $1/T$ varies less with ϵ for the as-measured data, Figs. 16 and 17. This results in a greater slope (Q_{DEF}/R) and higher values of Q_{DEF} from as-measured data. Thus, Q_{DEF} is overestimated from the as-measured data.

Figure 18 and 19 show the variation in Q_{DEF} with T , obtained from Table VI and Figs. 16 and 17, for the three strain rates studied, at an applied ϵ of 0.2 and 0.6, respectively. At the

lower $\dot{\epsilon}$, Fig. 18, values for Q_{DEF} from the two sets of data, as-measured and isothermal, are very similar, as expected from the similarity of the σ - ϵ data. More importantly, Figure 18 shows that Q_{DEF} varies significantly with T and in a much different fashion depending on $\dot{\epsilon}$. For a $\dot{\epsilon}$ of 1 s^{-1} , Q_{DEF} decreases with T . Conversely, at 0.01 s^{-1} it increases. At 1100°K , Q_{DEF} for high and low $\dot{\epsilon}$ have corresponding high and low values, 700 kJ/mole and 250 kJ/mole, respectively. At the intermediate $\dot{\epsilon}$, 0.1 s^{-1} , Q_{DEF} first decreases and then increases with increase in T . The three curves appears to converge near a value of 400 kJ/mole as T approaches 1400°K .

Figure 19 shows that at a $\dot{\epsilon}$ of 0.6, the variation in Q_{DEF} with T from the isothermal σ - ϵ data is well behaved, similar to the behavior shown in Figure 18 for lower $\dot{\epsilon}$. At 1100°K , Q_{DEF} increases significantly with $\dot{\epsilon}$, having a value of 270 kJ/mole at the lowest rate and 525 kJ/mole at the highest. As T increases, Q_{DEF} for the three strain rates converges to a value of approximately 375 to 400 kJ/mole at 1400°K . In contrast, the variation in Q_{DEF} calculated from the as-measured σ - ϵ data (dashed curves in Figure 19) shows no consistent behavior.

Variations in the value of Q_{DEF} with $\dot{\epsilon}$ could be attributed to a changing activity of the various dislocation mechanisms contributing to flow. For example, work hardening moderated by cross slip is probably the dominant mechanism at high $\dot{\epsilon}$ and low T . Dislocation climb and polygonization contribute to dynamic recovery at the low $\dot{\epsilon}$ and high T , similar to creep. A decrease

in Q_{DEF} with increase in T , similar to that observed in Figure 18 and 19 for a $\dot{\epsilon}$ of 1 s^{-1} would be expected and could be explained by increased thermal activation for dislocations to overcome short range barriers which obstruct their motion. However, the increase in Q_{DEF} observed at the lowest $\dot{\epsilon}$, 0.01 s^{-1} , is not readily expected in light of increased thermal activation at greater T but could be explained by a decreased dislocation mobility, e.g. reduced climb through dislocation pinning by individual solute atoms or atom-complexes. A similar increase in Q_{DEF} with T has been observed for creep of aluminum below $T/T_m=0.5$ and at a $\dot{\epsilon}$ of $3 \times 10^{-11} \text{ s}^{-1}$. The increase has been related to the transition from one deformation mechanism to another. At low T/T_m , creep is controlled by dislocation intersection processes; at intermediate values by cross slip of screw dislocations; and at higher values approaching 0.5 by dislocation climb and the nonconservative motion of jogs in screw dislocations.^{20,21} Above 0.5 T/T_m creep is entirely diffusion controlled and Q_{DEF} is relatively constant, increasing only slightly with T . However, as $\dot{\epsilon}$ is increased to a value of 0.03 s^{-1} , a rate similar to the slowest employed in this investigation, Q_{DEF} was shown to increase rapidly with T up to about 0.75 T/T_m . This is because comparatively little time is available at this higher $\dot{\epsilon}$ for diffusion controlled processes and the sensitivity of Q_{DEF} to T at low T/T_m is extended to higher T/T_m . The increase in Q_{DEF} with T for aluminum is similar to that observed here for 304L, both alloys deformed at equivalent $\dot{\epsilon}$ and T/T_m .

The value of Q_{DEF} for a $\dot{\epsilon}$ of 0.01 s^{-1} and T of 1100°K , 270 kcal/mole is significantly less than any of the values obtained by assuming an average linear behavior for the variation of Q_{DEF}/R for any σ level in Fig.15, and is in fair agreement with the value of 314 kJ/mole reported for creep of alloy 304.²² Similarly, Afonja²³ measured Q_{DEF} in a 23.6 Cr-5.12 Ni duplex stainless steel at a $\dot{\epsilon}$ of 0.01 s^{-1} and found the value, 242 kJ/mole , to agree with the activation energy reported for self diffusion in similar Fe-Cr-Ni alloys. Q_{creep} is generally equal to $Q_{self \text{ diffusion}}$.²² This suggests that Q_{DEF} for the creep realm may apply up to a $\dot{\epsilon}$ of 0.01 s^{-1} , a few orders of magnitude above that considered to be the upper bound of the creep realm.

Assuming a linear behavior in Fig. 17, Q_{DEF} from the as-measured σ - $\dot{\epsilon}$ data is about 370 kJ/mole at 100 MPa and 450 kJ/mole at 300 MPa , with Q_{DEF} increasing approximately linearly with σ . From the isothermal data, Q_{DEF} is relatively constant, having values which range between 346 and 370 kJ/mole for the range of σ considered. For 304- and 304L-type alloys values of Q_{DEF} ranging between 393 and 600 kJ/mole have been reported.¹⁵ It is probably more appropriate to assume that Q_{DEF} varies with $\dot{\epsilon}$ which would allow the determination of a variable Q_{DEF} in the transition realm between hot working, where Q_{DEF} is relatively high, and creep, where it is low.^[12]

G. Estimation of Onset of Dynamic Recrystallization

The onset of dynamic recrystallization has been related to a peak in the σ - $\dot{\epsilon}$ curve and Sellars²⁴ subsequently expressed the

strain to the peak as a function of initial grain size, d_0 , and Z as follows:

$$\epsilon_p = kd_0^{0.5}Z^B \quad [6]$$

where k and B are constants. This type of relationship has been useful in the identification of a set of deformation parameters and microstructure favoring dynamic recrystallization, e.g. during high energy rate forging of 304L.¹⁵

Values of ϵ_p at various T and $\dot{\epsilon}$ are given in Table VII. Figure 20 shows the variation in $\log \epsilon_p$ with Z for the as-measured and the isothermal σ - ϵ data where Q_{DEF} was assumed to have the average values of 406 and 355 kJ/mole, respectively, from Table VII. Here Q_{DEF} is assumed independent of ϵ , $\dot{\epsilon}$, and T , even though the findings in this investigation indicate otherwise. As-measured ϵ_p is lower than isothermal ϵ_p because deformational heating progressively lowers σ with increasing ϵ . In the case of dynamic recrystallization, the peak occurs prematurely. As a result, the as-measured data gives a significant underestimation of ϵ_p for any combination of $\dot{\epsilon}$ and T , or for any fixed value of Z .

Figure 20 shows that a unique relationship was not obtained for either of the two sets of data. The as-measured behaviors are grouped by $\dot{\epsilon}$ but have distinctly different slopes. The isothermal behaviors exhibit equal slope but separate according to $\dot{\epsilon}$. In the latter case, the separation between the curves is about an order of magnitude, in Z , which corresponds directly to the difference between the magnitude of the strain rates

employed. Figure 21 shows that the behavior of the isothermal data can be expressed by a single equation if the power on ϵ in Z is set to a value of 2 rather than 1 as follows,

$$Z_{\text{modified}} = \epsilon^2 \exp(Q_{\text{DEF}}/RT) \quad [7]$$

Assuming that Q_{DEF} varies with the deformation parameters ϵ , $\dot{\epsilon}$, and T, it can be calculated at each ϵ_p by linear interpolation of data in Table VI. Plots similar to Figures 20 and 21 (not shown) employing a variable Q_{DEF} shows no correlation between ϵ_p and Z. However, considering utilization of a Q_{DEF} which varies with ϵ and T, the relationship between ϵ_p and Z may simply reduce to one between ϵ_p and Q_{DEF} . Figure 22 shows that the variation ϵ_p with $\log Q_{\text{DEF}}$ is linear with a slope of -2. Thus ϵ_p is proportional to the inverse of Q_{DEF} squared. The data separates slightly according to $\dot{\epsilon}$. Figure 23 shows that the behavior is unified by inclusion of a $\dot{\epsilon}$ factor as follows,

$$\epsilon_p = A \dot{\epsilon}^{0.2} / Q_{\text{DEF}}^2 \quad [8]$$

where A is equal to 1.015×10^5 mole sec/kJ. Thus, it appears that the effect of $\dot{\epsilon}$ and T on ϵ_p can be taken into account, in part and totally, respectively, through the use of a Q_{DEF} which varies with $\dot{\epsilon}$ and T. Assuming Q_{DEF} is invariant with $\dot{\epsilon}$ and T necessitates the inclusion of $\dot{\epsilon}$ and T terms, via Z, in the analysis, as shown in Figures 20 and 21.

IV. DISCUSSION

The effect of test sample heating during conventional compression testing, in the $\dot{\epsilon}$ realm where deformational heat is neither fully conducted to the environment (i.e. isothermal

condition) nor fully retained by the test specimen (i.e. adiabatic condition), has been shown to be significant and should be considered in the interpretation and utilization of as-measured σ - ϵ data. For example, m from as-measured σ - ϵ data was found to be under estimated compared to m from the isothermal data. From the isothermal data, Q_{DEF} was found to increase with ϵ , a behavior that is consistent with the gradual transition from a low value for Q_{DEF} in the creep range to a higher one in the hot working range. The ϵ range studied here appears to comprise part of transition realm between hot working and creep. Deformational heating in the ϵ range studied here affects peak stress, progressively reducing the as-measured value compared to the corresponding isothermal value as ϵ is increased. Values for Q_{DEF} determined from peak stress values are over estimated from the as-measured data. The Q_{DEF} from isothermal data was found to increase with T at low ϵ and decrease at high ϵ . The former behavior could be explained by increased solute pinning of dislocations with increase in T , while the latter is consistent with an increased thermal activation for dislocation motion.

Correction for deformational heating of test samples, if applied to the as-measured data, would affect the analysis of a number of investigators.²⁵⁻³⁸ For example, Sample *et al.*²⁵, used similar compression sample size and testing techniques to study dynamic softening in copper and observed a sharp peak in the flow curve followed by a large stress drop which was followed by numerous, successively smaller peaks at a $\dot{\epsilon}$ of 0.005 s^{-1} and T of

700°C. At higher $\dot{\epsilon}$, 0.158 s⁻¹ a single broad peak was observed without subsequent oscillation. Sample et al. point out that as $\dot{\epsilon}$ increases from 0.005 s⁻¹ to 0.158 s⁻¹, the onset of dynamic recrystallization changes from corresponding precisely to ϵ_p to some critical level of ϵ , ϵ_c , that is less than the peak strain. The results of this investigation demonstrate that sample heating could account for, at least in part, the observed transition. At the lower $\dot{\epsilon}$ of 0.005 s⁻¹, the test can be considered to be nearly isothermal and assuming strain is distributed uniformly throughout the sample, the whole sample would undergo recrystallization at the same time, or value of ϵ , and a sharp drop in σ would be expected. However, at 0.158 s⁻¹, some of the heat of deformation would be retained and sample T increases with applied $\dot{\epsilon}$. In fact, a gradient in T, with T being the greatest at the sample interior and the least at the sample face in contact with the compression die, would exist as demonstrated in this study. Thus, dynamic recrystallization would start preferentially at the sample interior and progress toward the faces in contact with the dies and a broader, more diffuse peak in the flow curve, observed by Sample et al., should be expected.

The transition from single peak to multiple peak behavior has been interpreted by Jonas and Sakai²⁶ in terms of the ranking of the unrecrystallized (U) and recrystallized grain size (R):

(a) if $U \gg R$, a single broad peak is observed (because recrystallization occurs gradually by the repetitive nucleation of successive adjacent necklaces, initially forming at the

original high angle grain boundaries and afterward advancing into and consuming the worked grain interior), and (b) if $U < 2R$, a sharp large peak followed by smaller successive peaks are observed (because recrystallized grains which nucleate on opposite sides of a single cold worked grain impinge on each other, consuming the entire worked grain interior without further nucleation). In the latter case, the sample recrystallizes fully and rapidly once the critical strain for recrystallization, ϵ_c , is applied, causing a sharp drop in σ . Upon further straining, the sample can recrystallize repetitively giving additional oscillations in the flow curve as long as the recrystallization process from point to point in the sample remains in phase. The amplitude of the oscillations will eventually dampen as phase coherency degenerates. This transition from a single sharp peak to a diffuse single peak has been widely observed in the literature and discussed only in terms of the effect of the testing parameters, ϵ and T , and the initial microstructure. However, it is apparent that the effect of sample heating during deformation must also be considered.

Sample *et al.*²⁵ calculated Q_{DEF} for copper, by the procedure used in this investigation, and found it to vary significantly, having an average value of 237 kJ/mole. Strain rates were varied from 0.02 s^{-1} to 20 s^{-1} . Review of their data (Fig. 7 in reference) shows that if a temperature correction is applied to the as-measured σ - ϵ data, Q_{DEF} would vary less widely over the ϵ range tested and would have significantly lower values overall,

similar to the present findings for 304L.

Luton and Sellars²⁷ observed test sample heating in torsion of nickel, however, did not provide a correction in subsequent analysis of the σ - ϵ data. Q_{DEF} associated with the onset of dynamic recrystallization was calculated from the peak stress in the as-measured flow curves determined at strain rates between 0.002 s^{-1} and 4 s^{-1} and T between 762°C and 1249°C and by assuming Q_{DEF} invariant with ϵ and T . First, if a correction were applied to the as-measured flow curves for test sample heating, one would expect the isothermal peak stress would differ from the as-measured peak stress and that the difference would increase with ϵ . At the lowest ϵ , 0.002 s^{-1} , the two values would be nearly equal but at 4 s^{-1} the difference would be significant. This would result in a lower Q_{DEF} than reported, 234 kJ/mole , at least in the regime of lower T and higher ϵ where sample heating is expected to be the greatest. In fact, Luton and Sellars pointed out that Q_{DEF} calculated in their investigation was greater than was reported for recrystallization during creep in a nickel of similar purity. The noted discrepancy could be accounted for, at least in part, by considering sample heating during testing.

Staker and Grant²⁸ investigated microstructural changes during elevated T compression testing of alloy 305 stainless steel in the ϵ regime of 0.01 s^{-1} to 10 s^{-1} . In this study, volume-pct recrystallized and recrystallized grain size were measured as a function of hold time after deformation at T . However, T increases during compression and the as-measured

volume-pct recrystallized and recrystallized grain size is probably greater, at short hold times, than would be obtained from an isothermal test because the T increase in the test sample provides significant additional driving force for recrystallization. Further, as hold time is increased, the test sample, initially heated by deformation, cools to the initial T of the test, the furnace T, and one might expect that the volume-pct recrystallized and recrystallized grain size, in this case, would be more closely associated with the initial test T as hold time increases. However, Laasraoui and Jonas¹¹ estimated that the difference in the values for static fractional softening, corrected and uncorrected for deformational heating, obtained from interrupted compression testing of low carbon steels increases, rather than decreases with time at T. Thus, it appears that sample heating has a significant long term effect and must be considered in the determination of recrystallization kinetics or formulations which represent the effect of hot working parameters on microstructural features like volume-pct recrystallized and recrystallized grain size.

Samuel and Lalli²⁹ developed a viscoplastic constitutive model for the prediction of flow curves and evolution of hardness in aluminum deformed at elevated T. The constitutive parameters were calculated from as-measured σ - ϵ data obtained by compression testing conducted in the $\dot{\epsilon}$ realm of 0.05 s^{-1} to 10 s^{-1} . Although the samples employed were larger in size (as sample size increases, the $\dot{\epsilon}$ for isothermal testing is reduced) than those

employed in this study and by Charpentier *et al.*¹⁴ and so should have been subject to significant increases in sample T at strain rates greater than 0.1 s^{-1} , the authors apparently made no correction to the as-measured σ - ϵ data to compensate for sample heating and the associated softening. In their study the measured curves differ from model predictions, the former showing relatively more softening with increasing strain (Figs. 14 and 16 in reference) which would be consistent with an increase in T in the test sample, due to deformational heating, with increase in ϵ . The lack of softening in the predicted curves, presented by the authors, appears to be consistent with the proposed model which did not account for deformational heating of the test sample. Models like this one are certainly useful for predicting the evolution of flow stress and hardness during hot working. However, a correction to the as-measured σ - ϵ data for deformational heating would give a more accurate representation of material behavior. Such correction is certainly warranted should the data be used in conjunction with advanced simulative techniques, such as FEA, which can provide accurate, cost saving analysis. Ultimate success of these techniques depends, in part, on accurate definitions of material behavior.

Finally, Raj³⁰ presented hypothetical processing maps for use in warm-forming and hot-forming processes in which areas for dynamic recrystallization and flow localization due to deformational heating were shown as a function of $\dot{\epsilon}$ and T, where the minimum $\dot{\epsilon}$ for concern was shown to be approximately 1 s^{-1} .

The results of this investigation show that the minimum $\dot{\epsilon}$ level in such maps should probably be reduced by at least by an order of magnitude, to 0.1 s^{-1} , for small test specimens and more for larger work pieces. A similar observation is made for the processing maps presented by Gandhi³¹.

V. CONCLUSIONS

1. Although 304L test sample, dies, and environment are at the same T at the start of the compression test, the test sample can undergo significant heating in the $\dot{\epsilon}$ range from 0.01 s^{-1} to 1 s^{-1} . As-measured σ - ϵ data is significantly affected and should be corrected for these excursions in T to obtain the isothermal behavior.
2. The T of 304L compression specimens was found by FEA to vary nonlinearly with ϵ and $\dot{\epsilon}$, making the determination of isothermal σ - ϵ behavior from the as-measured one a nontrivial task. Heat conduction from the test sample, heated by deformation, to the cooler dies moderates the increase in sample T that would be calculated by conventional methods for an adiabatic test condition.
3. Values for various hot working parameters, e.g. m , Q_{DEF} , and ϵ_p , are significantly affected by the type of data, as-measured or isothermal σ - ϵ data, used in their calculation.
4. The transition of a flow curve exhibiting a sharp peak to one with a broad peak with increase in $\dot{\epsilon}$, where the occurrence of the peak is attributed to the onset of dynamic recrystallization, may

be due in part to the transition from an isothermal state in the test sample at lower ϵ to one where sample T increases with ϵ due to the heat associated with deformation. In the former, recrystallization proceeds in-phase throughout the sample, assuming a uniform distribution of ϵ and fine grain size in the sample. In the latter recrystallization initiates preferentially at the sample interior because of the locally higher T. Thus, recrystallization proceeds out-of-phase in the sample which should have a broadening effect on the peak in the flow curve.

5. The method of Thomas and Shrinivasan is appropriate for correcting as-measured σ - ϵ data for deformational heating of the test sample only for materials which develop a steady state σ , i.e. materials with high SFE. For other materials, FEA of the test is recommended, at least in the ϵ realm where the test condition is neither adiabatic nor isothermal.

ACKNOWLEDGEMENTS

This work was performed under contract with the United States Department of Energy. The authors would like to acknowledge the technical support received from Michael Riendeau and Gary Coubrough, during mechanical testing, and Michael Weis, graduate student at the Advanced Steel Processing and Products Research Center, Colorado School of Mines, Golden, CO., for help in constructing the compression testing system.

REFERENCES

1. S. Kobayashi, S.I. Oh, and T. Altan: *Metal Forming and the Finite-Element-Method*, Oxford University Press, New York, N.Y., 1989.
2. C.R. Boer, N. Rebelo, H. Rydstad, G. Schroder: *Process Modelling of Metal Forming and Thermomechanical Treatment*, Springer-Verlag, Heidelberg, Germany, 1986.
3. I. Haque, J.E. Jackson, Jr., T. Gangjee, and A. Raikar: "Empirical and Finite Element Approaches to Forging Die Design: A State-of-the-Art Survey," *J. Mater. Shaping Technol.*, vol. 5, No. 1, 1987, pp. 23-33.
4. K.J. Meltsner: "Prediction of Microstructural Evolution Using Finite Element Analysis and Structure Development Rules," *Simulation and Theory of Evolving Microstructures and Textures*, eds. M.P. Anderson and A. Rollet, TMS, Warrendale, PA, 1990.
5. A.J.M. Shih and H.T.Y. Yang: "Eperimental and Finite Element Simulation Methods for Rate-Dependent Metal Forming Processes," *International Journal for Numei*, Vol. 31, 1991, pp. 345-367.
6. S.I. Oh, G.D. Lahoti, and T. Altan: "Application of a Rigid-Plastic Finite Element Method to Some Metal Forming Operations," in *Process Modeling Tools*, Proceedings of American Society for Metals Process Modeling Sessions, Materials & Processes Congress, 1980, ASM, Metals Park, Ohio, 1981, pp. 195-216.
7. Semiatin, S. L., Lahoti, G. D., and Altan, T.: "Determination and Analysis of Flow Stress Data for Ti-6242 at Hot Working

Temperatures," *Process Modeling: Fundamentals and Applications to Metals*, coordinated by T. Altan, ASM, Metals Park, Ohio, 1980, p 387.

8. D.W. Livesey and C. M. Sellars: "Hot-deformation Characteristics of Waspaloy," *Mats. Sci. and Technology*, Feb. 1985, vol. 1, pp. 136-144.

9. A. Laasraoui and J.J. Jonas: "Recrystallization of Austenite after Deformation at High Temperatures and Strain Rates-- Analysis and Modeling," *Metall. Trans. A*, vol. 22A, Jan., 1991, pp. 151-160.

10. A. Laasraoui and J.J. Jonas: "Prediction of Steel Flow Stresses at High Temperatures and Strain Rates," *Metall. Trans. A*, vol. 22A, July, 1991, pp. 1545-1558.

11. Douglas, J. R., and Altan, T., "Flow Stress Determination for Metals at Forging Rates and Temperatures," *ASME Transactions, J. Engr. for Industry*, February 1975, p. 66.

12. K.P. Rao, S.M. Doraivelu, and V. Gopinathan: "Flow Curves and Deformation of Materials at Different Temperatures and Strain Rates," *J. Mechanical Working Technology*, no. 6, 1982, pp. 63-88.

13. J.F. Thomas, Jr., and R. Shrinivasan: "Constitutive Equations for High-Temperature Deformation," in *Computer Simulation in Materials Science*, eds. R.J. Arsenault, J.R. Beeler, Jr., and D.M. Esterling, ASM, Metals Park, OH, 1988, pp. 269-290.

14. P.L. Charpentier, B.C. Stone, S.C. Ernst, and J.F. Thomas, Jr.: "Characterization and Modeling of the High Temperature Flow Behavior of Aluminum Alloy 2024," *Metall. Trans. A*, vol. 17A,

Dec. 1986, pp. 2227-2237.

15. M.C. Mataya, E.L. Brown, and M.P. Riendeau: "Effect of Hot Working on Structure and Strength of Type 304L Austenitic Stainless Steel," *Metall. Trans. A*, vol. 21A, no. 7, July, 1990. pp. 1969-1987.

16. H. J. McQueen and J. J. Jonas: "Recent Advances in Hot Working: Fundamental Dynamic Softening Mechanisms," *J. Applied Metalworking*, vol. 3, No. 3, July 1984, pp. 233-241.

17. W. Reiss and K. Pohlandt: "The Rastegaev Upset Test-A Method to Compress Large Material Volumes Homogeneously," *Experimental Techniques*, January, 1986, pp. 20-24.

18. M.J. Weis: "The Hot Deformation Behavior of As-Cast Alloy 718," M.S. Thesis, no. T-3382, Colorado School of Mines, Golden, CO, 1987.

19. C. Zener and J.H. Hollomon: "Effect of Strain Rate Upon Plastic Flow of Steel," *J. of Applied Physics*, vol. 15, Jan., 1944, pp. 22-31.

20. O.D. Sherby and P.M. Burke: "Mechanical Behavior of Crystalline Solids at Elevated Temperature," in *Progress in Materials Science*, Vol. 13, eds. B. Chalmers and W. Hume-Tothery, Pergamon Press, London, England, 1968, pp. 325-353.

21. H. Luthy, A.K. Miller, and O.D. Sherby: "The Stress and Temperature Dependence of Steady-State Flow at Intermediate Temperatures for Pure Polycrystalline Aluminum," *Acta Met.*, vol. 28, 1980, pp. 169-178.

22. H.J. McQueen: "Deformation Mechanisms in Hot Working," *Jour.*

of Metals, April, 1968, pp. 31-38.

23. A.A. Afonja: "Grain Size Dependence of the Strain Rate Sensitivity and Activation Energy of High Temperature Deformation of a Microduplex Stainless Steel," *Matls. Sci and Engineering*, no. 54, 1982, pp. 257-263.

24. C.M. Sellars: in *Hot Working and Forming Processes*, Proc. Conf., Sheffield, England, July 1979, Metals Society, London, 1980, pp. 3-15.

25. V. M. Sample, G. L. Fitzsimons, and A. J. DeArdo: Dynamic Softening of Copper During Deformation at High Temperatures and Strain Rates," *Acta metall.*, Vol. 35, No. 2, 1987, pp. 367-379.

26. J. J. Jonas and T. Sakai: "A New Approach to Dynamic Recrystallization," in *Deformation Processing and Structure*, ed. G. Krauss, ASM, Metals Park, Ohio, 1982, pp. 185-230.

27. J. J. Luton and C. M. Sellars: "Dynamic Recrystallization in Nickel and Nickel Iron Alloys During High Temperature Deformation," *Acta Metallurgica*, Vol. 17, August 1969, pp. 1033-1043.

28. M.R. Staker and N.J. Grant: "The Effects of Strain, Strain Rate and Temperature on Grain Refinement and Hot Workability of Type 305 stainless Steel," *Matls. Sci and Engring*, no. 75, 1985, pp. 137-150.

29. V.M. Sample and L.A. Lalli: "Effects of Thermomechanical History on Hardness of Aluminum," *Matls. Sci. and Tech.*, Vol. 3, Jan. 1987, pp. 28-35.

30. R. Raj: "Development of a Processing Map for Use in Warm-

Forming and Hot-Forming Processes," *Metall. Trans. A.*, vol. 12A, June, 1981, pp. 1089-1097.

31. C. Gandhi: "On Fracture Initiation Mechanisms and Dynamic Recrystallization during Hot Deformation of Pure Nickel," *Metall. Trans. A*, vol. 13A, July, 1982, pp. 1233-1238.

32. W. Roberts, H. Boden, and B. Ahlblom: "Dynamic Recrystallization Kinetics", *Metal Sci.*, March-April, 1979, pp. 195-205.

33. M. J. White and W.S. Owen: "Effects of Vanadium and Nitrogen on Recovery and Recrystallization During and After Hot-Working Some HSLA Steels", *Metall. Trans. A*, Vol. 11A, April, 1980, pp. 597-604.

34. J.J. McQueen, G. Gurewitz and S. Fulop: "Influence of Dynamic Restoration Mechanisms on the Hot Workability of Waspaloy and Concentrated FCC Alloys", *High Temperature Technology*, Feb. 1983, pp. 131-138.

35. L.A. Norstrom: "Hot Ductility and Restoration in Two Highly Alloyed Austenitic Steels", *Scand. J. Metallurgy*, vol. 6, 1977, pp. 269-276.

36. H. Cederblad and N. J. Grant: "Hot Workability of Nimonic 115 as a Function of Strain Rate", *Metall. Trans A*, vol. 6A, Aug. 1975, pp. 1547-1552.

37. W. Roberts and B. Ahlblom: "A Nucleation Criterion for Dynamic Recrystallization During Hot Working", *Acta Met.*, vol. 26, 1978, pp. 801-813.

38. H.J. McQueen: "The Production and Utility of Recovered

Dislocation Substructures", *Metall. Trans. A*, vol. 8A, June 1977,
pp. 807-824.

LIST OF FIGURE CAPTIONS

Figure 1. Schematic of FEA model. Nodes on centerline axis are free to move along axis but not perpendicular to axis. Temperature of moving die is fixed at the initial test temperature. Imaginary die is located at mid-height of compression sample. Coefficient of friction between specimen and dies is zero.

Figure 2. The change in specimen temperature with true plastic strain for alloy 304L compressed at 950°C and a $\dot{\epsilon}$ of 0.1 s⁻¹. Both the as-measured (solid) and FEA (dashed) curves are shown. Curves A through F were generated with heat transfer (film) coefficients of 1.635, 4.905, 6.540, 8.175, 11.44, and 16.35 x 10³ J/sec/m²/°K, respectively. As-measured temperature data were obtained from an embedded thermocouple located at the center of the specimen.

Figure 3. The variation of true stress with initial deformation temperature of the compression test for three selected strain levels. Data points were selected from the as-measured stress-strain data for alloy 304L compressed at a $\dot{\epsilon}$ of 1 s⁻¹, at temperatures between 750°C and 1150°C.

Figure 4. The change in specimen temperature with true plastic strain for alloy 304L compressed at a $\dot{\epsilon}$ of 1 s⁻¹. The initial test temperatures, between 750°C and 1150°C,

are shown. Dashed curves were calculated by the method of Thomas and Shrinivasan¹³ and the solid curves are predicted by FEA.

Figure 5. The change in specimen temperature with true plastic strain for alloy 304L compressed at a $\dot{\epsilon}$ of 0.1 s^{-1} . The initial test temperatures, between 750°C and 1150°C , are shown. Dashed curves were calculated by the method of Thomas and Shrinivasan¹³ and the solid curves are predicted by FEA.

Figure 6. The change in specimen temperature with true plastic strain for alloy 304L compressed at a $\dot{\epsilon}$ of 0.01 s^{-1} . The initial test temperatures, between 750°C and 1150°C , are shown. Dashed curves were calculated by the method of Thomas and Shrinivasan¹³ and the solid curves are predicted by FEA.

Figure 7. The change in specimen temperature with true plastic strain for alloy 304L compressed at a $\dot{\epsilon}$ of 0.1 s^{-1} , at temperatures of 850°C and 950°C . Dashed curves were calculated by the method of Thomas and Shrinivasan¹³. The solid curves are predicted by FEA. The open symbols (squares) were measured via an embedded thermocouple located at the center of the test specimen.

Figure 8. True stress versus true plastic strain for alloy 304L compressed at a $\dot{\epsilon}$ of 1 s^{-1} . The initial temperature of the tests ranged between 750°C and 1150°C . Solid curves are the as-measured behavior. Dashed curves are

from the method of Thomas and Shrinivasan¹³. Solid curves with symbols (circles) are the isothermal curves from the FEA method.

Figure 9. True stress versus true plastic strain for alloy 304L compressed at a $\dot{\epsilon}$ of 0.1 s^{-1} . The initial temperature of the tests ranged between 750°C and 1150°C . Solid curves are the as-measured behavior. Dashed curves are from the method of Thomas and Shrinivasan¹³. Solid curves with symbols (circles) are the isothermal curves from the FEA method.

Figure 10. True stress versus true plastic strain for alloy 304L compressed at a $\dot{\epsilon}$ of 0.01 s^{-1} . The initial temperature of the tests ranged between 750°C and 1150°C . Solid curves are the as-measured behavior. Dashed curves are from the method of Thomas and Shrinivasan¹³. Solid curves with symbols (circles) are the isothermal curves from the FEA method.

Figure 11. Heat retention efficiency, η , versus $\log \dot{\epsilon}$ in the $\dot{\epsilon}$ realm where conventional sized compression test samples of alloy 304L exhibit neither an isothermal nor an adiabatic state. η for both methods, FEA and Thomas & Shrinivasan are shown. Note the η from FEA is dependent while that from Thomas & Shrinivasan is independent of the applied strain. Data for aluminum is from Charpentier et al.¹⁴

Figure 12. The variation of strain rate sensitivity, m , with the initial test temperature for alloy 304L compressed to a strain of 0.6. $M(L)$ is m calculated from the low $\dot{\epsilon}$ range, 0.01 s^{-1} to 0.1 s^{-1} ; $M(H)$ is from the high $\dot{\epsilon}$ range, 0.1 s^{-1} to 1 s^{-1} . Dashed curves were calculated from the as-measured stress-strain data while the solid curves are from the FEA isothermal data.

Figure 13. The variation of strain rate sensitivity, m , with true strain, for an initial test temperature of 950°C , for alloy 304L. $M(L)$ is m calculated for the low $\dot{\epsilon}$ range, 0.01 s^{-1} to 0.1 s^{-1} ; $M(H)$ is from the high $\dot{\epsilon}$ range, 0.1 s^{-1} to 1 s^{-1} . Dashed curves were calculated from the as-measured stress-strain data while the solid curves are from the FEA isothermal data.

Figure 14. The variation of true stress with inverse temperature (kelvin^{-1}) for alloy 304L compressed at three different strain rates to a true strain of 0.2. Dashed curves are from the as-measured stress-strain data. The solid curves are from FEA isothermal data. Values of inverse temperature at various constant stress levels from this figure are utilized in Fig. 16.

Figure 15. The variation of true stress with inverse temperature (kelvin^{-1}) for alloy 304L compressed at three different strain rates to a true strain of 0.6. Dashed curves are from the as-measured stress-strain data. The solid curves are from FEA isothermal data. Values of inverse

temperature at various constant stress levels from this figure are utilized in Fig. 17.

Figure 16. The variation in natural logarithm of strain rate with inverse temperature (kelvin^{-1}) at various constant stress levels, in MPa, for alloy 304L compressed to a strain of 0.2. Dashed curves are from the as-measured stress-strain data. The solid curves are from FEA isothermal data.

Figure 17. The variation in natural logarithm of strain rate with inverse temperature (kelvin^{-1}) at various constant stress levels, in MPa, for alloy 304L compressed to a strain of 0.6. Dashed curves are from the as-measured stress-strain data. The solid curves are from FEA isothermal data.

Figure 18. The variation of activation energy, Q_{DEF} , with initial deformation temperature for alloy 304L compressed at three different strain rates to strain of 0.2. Dashed curves are from the as-measured stress-strain data. The solid curves are from FEA isothermal data.

Figure 19. The variation of activation energy, Q_{DEF} , with initial deformation temperature for alloy 304L compressed at three different strain rates to strain of 0.6. Dashed curves are from the as-measured stress-strain data. The solid curves are from FEA isothermal data.

Figure 20. Variation of logarithm peak strain with logarithm Z for 304L deformed at three different strain rates.

Dashed curves originate from as-measured stress-strain data and Q_{DEF} in Z is assumed to have a constant value of 407 kJ/mole from Table VI. The solid curves are from FEA isothermal data and Q_{DEF} has a value of 356 kJ/mole from Table VI.

Figure 21. Variation of logarithm peak strain with logarithm $Z_{modified}$, where the power on strain rate in Z is 2 rather than 1, for 304L deformed at three different strain rates. Dashed curves originate from as-measured stress-strain data and Q_{DEF} in Z is assumed to have a constant value of 406 kJ/mole from Table VI. The solid curves are from FEA isothermal data and Q_{DEF} has a value of 355 kJ/mole from Table VI. Logarithm of peak strain versus logarithm of a modified Z.

Figure 22. Variation of logarithm peak strain with logarithm Q_{DEF} for 304L compressed at three different strain rates. Values for Q_{DEF} assumed to vary with strain rate and temperature, are listed in Table VI.

Figure 23. Variation of logarithm peak strain with logarithm $(\dot{\epsilon}^{-0.1}Q_{DEF})$ for 304L compressed at three different strain rates. Values for Q_{DEF} assumed to vary with strain rate and temperature, are listed in Table VI. Inclusion of the strain rate term, $\dot{\epsilon}^{-0.1}$, unifies the relationship, shown in Fig. 22. The unifying equation is $\epsilon_p = A\dot{\epsilon}^{0.2}/Q^2$, where $A = 1.015 \times 10^5$ mole sec/kJ.

LIST OF TABLE CAPTIONS

- Table I. Chemical Analysis of 304L Alloy.
- Table II. Variation of Young's modulus, thermal expansion coefficient, thermal conductivity, and specific heat with temperature and other constants used in the FEA model.
- Table III. The as-measured (MEAS) and FEA isothermal (ISO) values of stress for various deformation temperatures, at 0.1 increments of ϵ , and a $\dot{\epsilon}$ of 1 s^{-1} .
- Table I. The as-measured (MEAS) and FEA isothermal (ISO) values of stress for various deformation temperatures, at 0.1 increments of ϵ , and a $\dot{\epsilon}$ of 0.1 s^{-1} .
- Table V. The as-measured (MEAS) and FEA isothermal (ISO) values of stress for various deformation temperatures, at 0.1 increments of ϵ , and a $\dot{\epsilon}$ of 0.01 s^{-1} .
- Table VI. Activation energy, Q_{DEF} , at constant stress and for two strain levels, 0.2 and 0.6. Values are shown for two assumptions: Q_{DEF} varies with strain rate or is constant over the entire strain rate range.
- Table VII. Values for peak strain (ϵ_p) for fine grain 304L tested at various T- $\dot{\epsilon}$ pairs. Values from both as-measured and isothermal σ - ϵ data are given.

Table I. Chemical Analysis of 304L Alloy.

<u>Element</u>	<u>Analysis (wt. pct.)</u>
Cr	18.6
Mn	1.9
Ni	10.0
P	0.011
Si	0.57
Mo	0.055
Co	0.077
C	0.022
S	0.0003
N	0.015
Fe	Balance

Table II. Variation of Young's modulus, thermal expansion coefficient, thermal conductivity, and specific heat with temperature and other constants used in the FEA model.

T (°C)	YOUNG'S MODULUS (MPa) (x 10 ⁵)	THERMAL EXPANSION COEFFICIENT (cm/cm-°C) (x 10 ⁻⁵)	THERMAL CONDUCTIVITY (cal/sec-cm-°C) (x 10 ²)	SPECIFIC HEAT (cal/gm°C)
-17.8	1.998	1.507	3.52	0.089
93.3	1.950	1.613	4.02	0.090
204.4	1.895	1.699	4.34	0.091
315.6	1.667	1.768	4.68	0.093
426.7	1.481	1.823	4.96	0.095
537.8	1.247	1.868	5.29	0.098
648.9	9.440	1.908	5.66	0.104
760.0	7.440	1.946	6.00	0.109
871.1	6.340	1.980	6.32	0.113
982.2	5.170	2.011	6.66	0.115
1093.3	4.000	2.034	6.98	0.117

OTHER CONSTANTS:

DENSITY: 7.999 gm/cm³
 POISSON'S RATIO: 0.300
 MECHANICAL ENERGY TO HEAT:
 CONVERSION: 0.238978 cal/MPa-cm³
 95% EFFICIENCY: 0.227029 cal/MPa-cm³

Table III. The as-measured (MEAS) and FEA isothermal (ISO) values of stress for various deformation temperatures, at 0.1 increments of ϵ , and a $\dot{\epsilon}$ of 1 s^{-1} .

ϵ	750°C		850°C		950°C		1050°C		1150°C	
	<u>MEAS</u>	<u>ISO</u>								
0.0	78.4	78.4	78.1	78.1	75.5	75.5	59.7	59.7	50.4	50.4
0.1	236	238	206	207	171	172	114	115	83.5	83.9
0.2	289	294	247	251	198	202	130	134	93.1	94.5
0.3	317	326	267	275	210	218	138	144	99.0	101
0.4	334	349	278	291	217	229	142	151	102	106
0.5	344	366	285	303	221	237	143	156	103	108
0.6	351	381	287	313	222	243	142	159	102	108
0.7	355	395	288	320	222	247	140	160	101	107
0.8	357	406	286	326	220	249	136	160	98.3	105
0.9	358	418	283	332	218	251	132	160	95.7	103
1.0	358	430	280	338	214	252	127	159	93.2	101

Table IV. The as-measured (MEAS) and FEA isothermal (ISO) values of stress for various deformation temperatures, at 0.1 increments of ϵ , and a $\dot{\epsilon}$ of 0.1 s^{-1} .

ϵ	750°C		850°C		950°C		1050°C		1150°C	
	<u>MEAS</u>	<u>ISO</u>								
0.0	96.6	96.6	84.0	84.0	78.4	78.4	58.0	58.0	35.7	35.7
0.1	233	235	192	193	134	135	87.9	88.7	57.1	57.4
0.2	278	284	222	226	150	155	99.0	101	64.4	65.3
0.3	300	311	236	245	158	166	104	108	68.3	69.7
0.4	313	329	243	256	163	174	106	110	67.6	69.5
0.5	320	342	246	263	165	177	104	110	64.3	66.6
0.6	325	350	247	266	164	178	99.3	106	61.5	63.9
0.7	328	356	247	268	161	176	95.4	102	60.0	62.3
0.8	331	360	246	268	157	172	92.8	99.5	58.7	60.8
0.9	333	363	244	267	153	168	90.6	96.7	57.4	59.4
1.0	335	363	246	267	150	164	89.0	94.4	56.7	58.4

Table V. The as-measured (MEAS) and FEA isothermal (ISO) values of stress for various deformation temperatures, at 0.1 increments of ϵ , and a $\dot{\epsilon}$ of 0.01 s^{-1} .

ϵ	750°C		850°C		950°C		1050°C		1150°C	
	MEAS	ISO	MEAS	ISO	MEAS	ISO	MEAS	ISO	MEAS	ISO
0.0	102	102	93.9	93.9	64.2	64.2	44.8	44.8	23.2	23.2
0.1	214	216	150	152	96.1	96.8	62.0	62.3	39.6	39.7
0.2	250	253	169	171	108	109	70.6	71.1	45.8	46.0
0.3	267	272	179	182	114	116	72.0	72.6	42.7	42.9
0.4	278	283	186	188	117	118	63.7	64.3	40.6	40.8
0.5	286	290	188	191	114	116	62.5	63.0	40.6	40.7
0.6	291	295	189	192	110	112	63.7	64.1	39.5	39.6
0.7	295	298	189	191	107	108	62.4	62.7	39.3	39.4
0.8	298	301	188	190	104	105	61.0	61.2	39.0	39.0
0.9	300	303	188	189	103	104	61.3	61.5	38.6	38.6
1.0	301	304	187	189	101	102	61.5	61.7	38.7	38.7

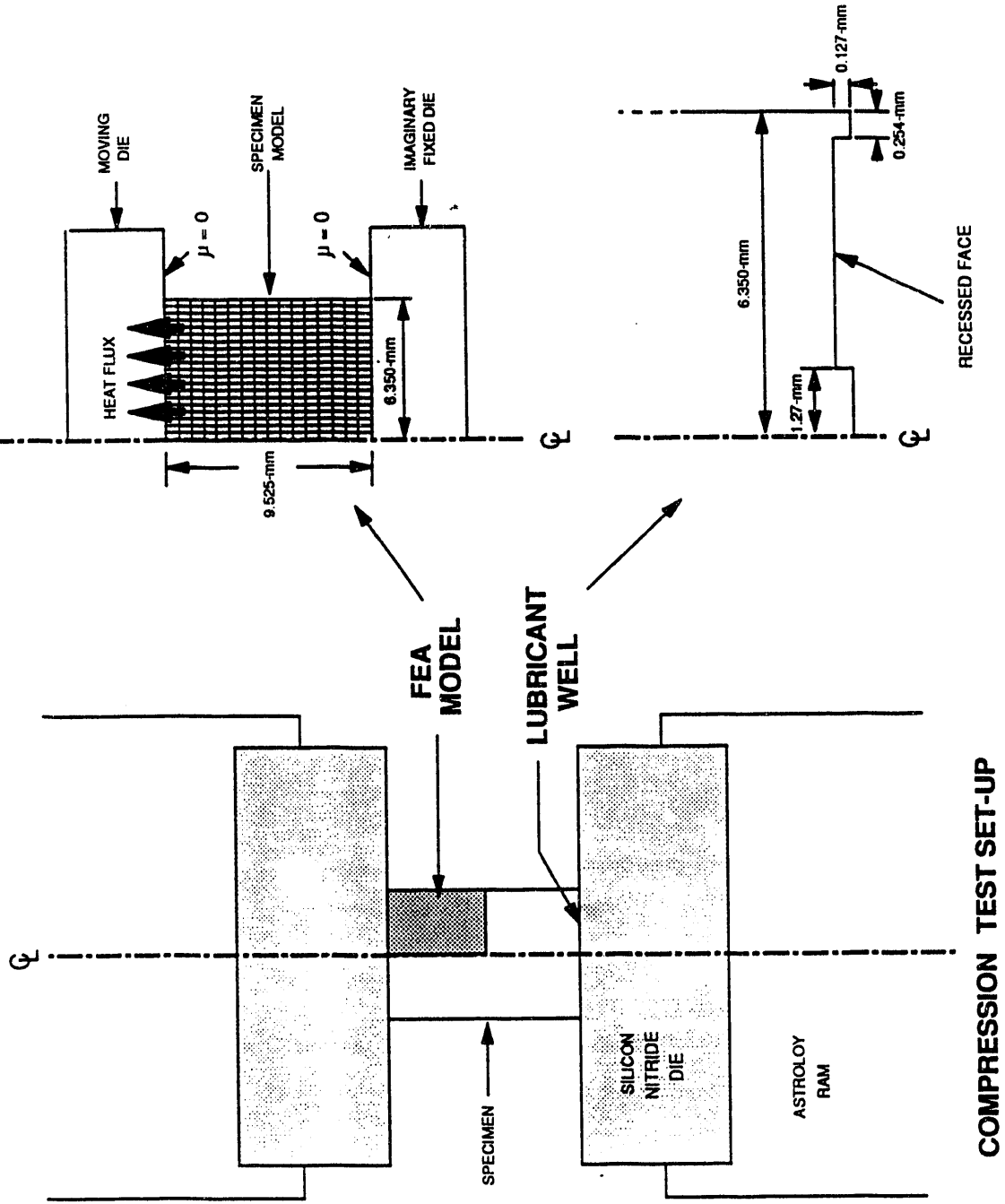
Table VI. Activation energy, Q_{DEF} , at constant stress and for two strain levels, 0.2 and 0.6. Values are shown for two assumptions: Q_{DEF} varies with strain rate or is constant over the entire strain rate range.

<u>Stress (MPa)</u>	<u>Activation Energy, kJ/mole</u>							
	<u>Variable</u>						<u>Invariable</u>	
	<u>1 s⁻¹</u>		<u>0.1 s⁻¹</u>		<u>0.01 s⁻¹</u>			
	<u>MEAS</u>	<u>ISO</u>	<u>MEAS</u>	<u>ISO</u>	<u>MEAS</u>	<u>ISO</u>	<u>MEAS</u>	<u>ISO</u>
100								
Strain=0.2	441	450	422	417	402	381	---	---
Strain=0.6	340	400	373	363	402	321	372	358
150								
Strain=0.2	470	469	399	394	312	302	---	---
Strain=0.6	408	389	386	347	364	300	386	346
200								
Strain=0.2	534	544	418	418	254	233	---	---
Strain=0.6	446	414	403	352	356	277	404	348
250								
Strain=0.2	609	658	471	488	271	204	---	---
Strain=0.6	478	457	423	366	361	245	422	358
300								
Strain=0.2	---	---	---	---	---	---	---	---
Strain=0.6	449	485	449	381	449	234	<u>450</u>	<u>370</u>
							AVERAGE=	407 356

Table VII. Values for peak strain (ϵ_p) for fine grain 304L tested at various T- $\dot{\epsilon}$ pairs. Values from both as-measured and isothermal σ - ϵ data are given.

$\dot{\epsilon}$	<u>750°C</u>	<u>850°C</u>	<u>950°C</u>	<u>1050°C</u>	<u>1150°C</u>
0.01 s⁻¹					
As-measured	>1.0	0.60	0.40	0.26	0.23
Isothermal	>1.0	0.55	0.40	0.25	0.20
0.1 s⁻¹					
As-measured	>0.85	0.61	0.51	0.38	0.34
Isothermal	>1.0	0.75	0.56	0.44	0.35
1.0 s⁻¹					
As-measured	>0.86	0.65	0.61	0.51	0.50
Isothermal	>1.0	>1.0	>1.0	0.76	0.57

Figure 1. Schematic of FEA model. Nodes on centerline axis are free to move along axis but not perpendicular to axis. Temperature of moving die is fixed at the initial test temperature. Imaginary die is located at mid-height of compression sample. Coefficient of friction between specimen and dies is zero.



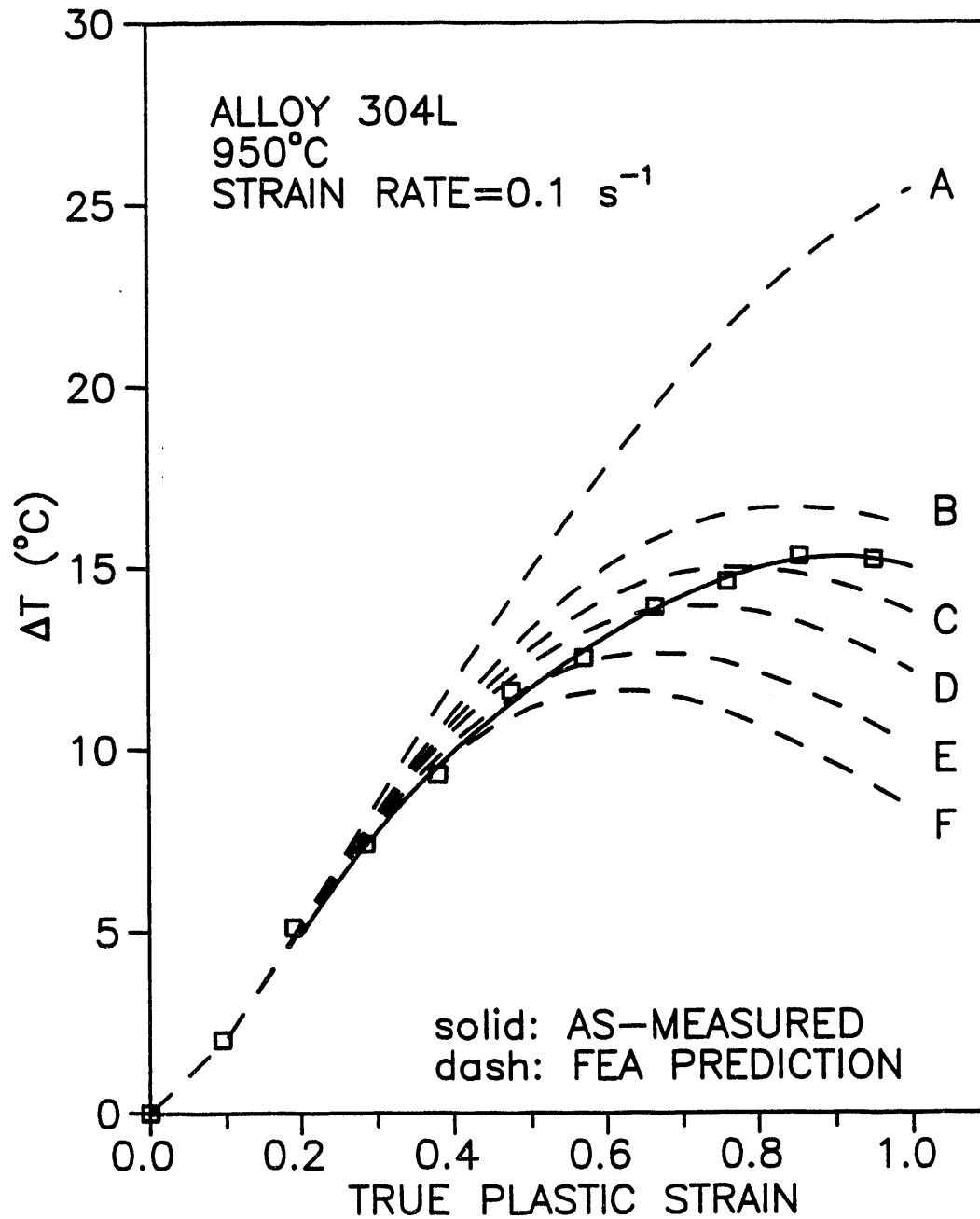


Figure 2. The change in specimen temperature with true plastic strain for alloy 304L compressed at 950°C and a $\dot{\epsilon}$ of 0.1 s⁻¹. Both the as-measured (solid) and FEA (dashed) curves are shown. Curves A through F were generated with heat transfer (film) coefficients of 1.635, 4.905, 6.540, 8.175, 11.44, and 16.35 x 10³ J/sec/m²/°K, respectively. As-measured temperature data were obtained from an embedded thermocouple located at the center of the specimen.

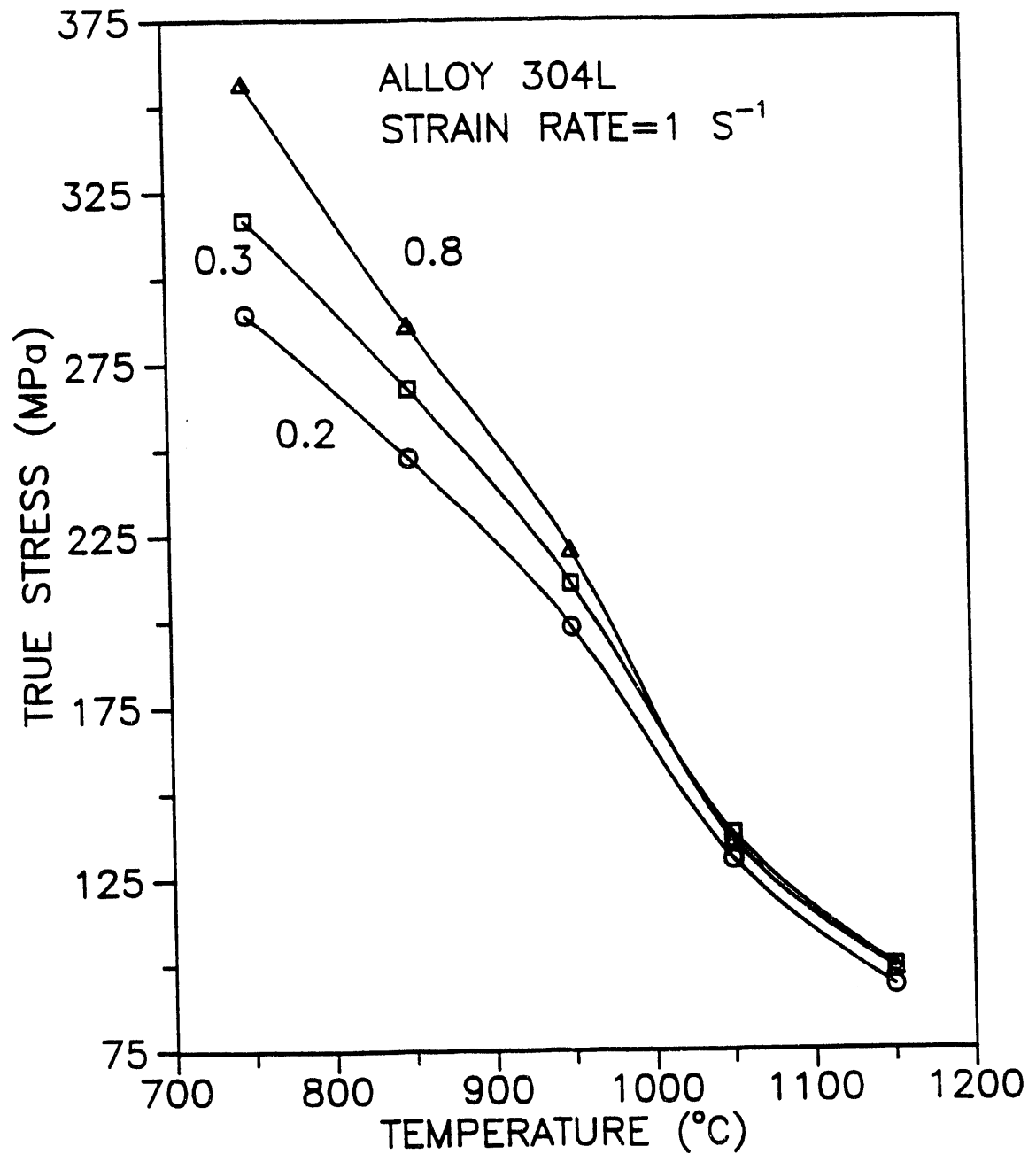


Figure 3. The variation of true stress with initial deformation temperature of the compression test for three selected strain levels. Data points were selected from the as-measured stress-strain data for alloy 304L compressed at a $\dot{\epsilon}$ of 1 s⁻¹, at temperatures between 750°C and 1150°C.

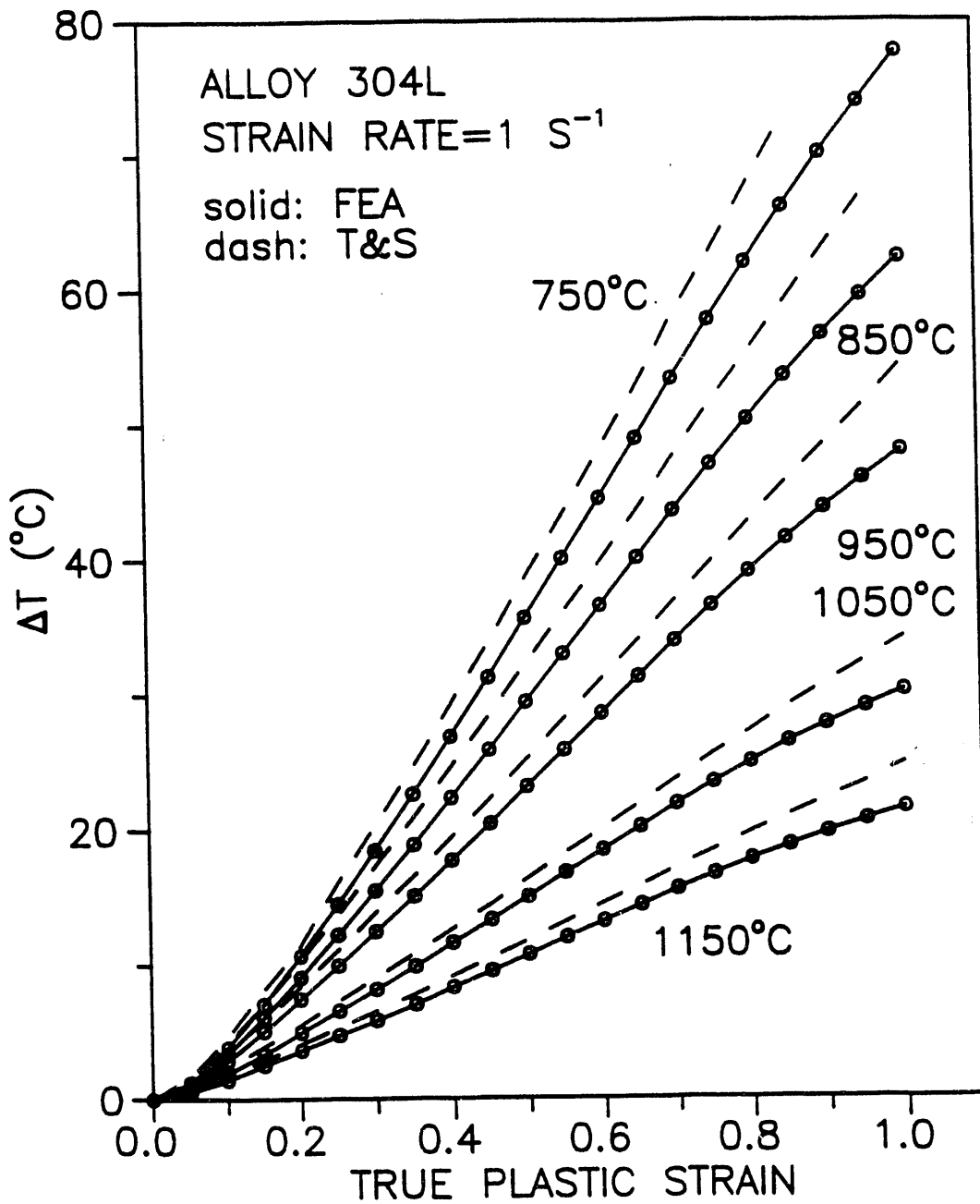


Figure 4. The change in specimen temperature with true plastic strain for alloy 304L compressed at a $\dot{\epsilon}$ of 1 s⁻¹. The initial test temperatures, between 750°C and 1150°C, are shown. Dashed curves were calculated by the method of Thomas and Shrinivasan¹³ and the solid curves are predicted by FEA.

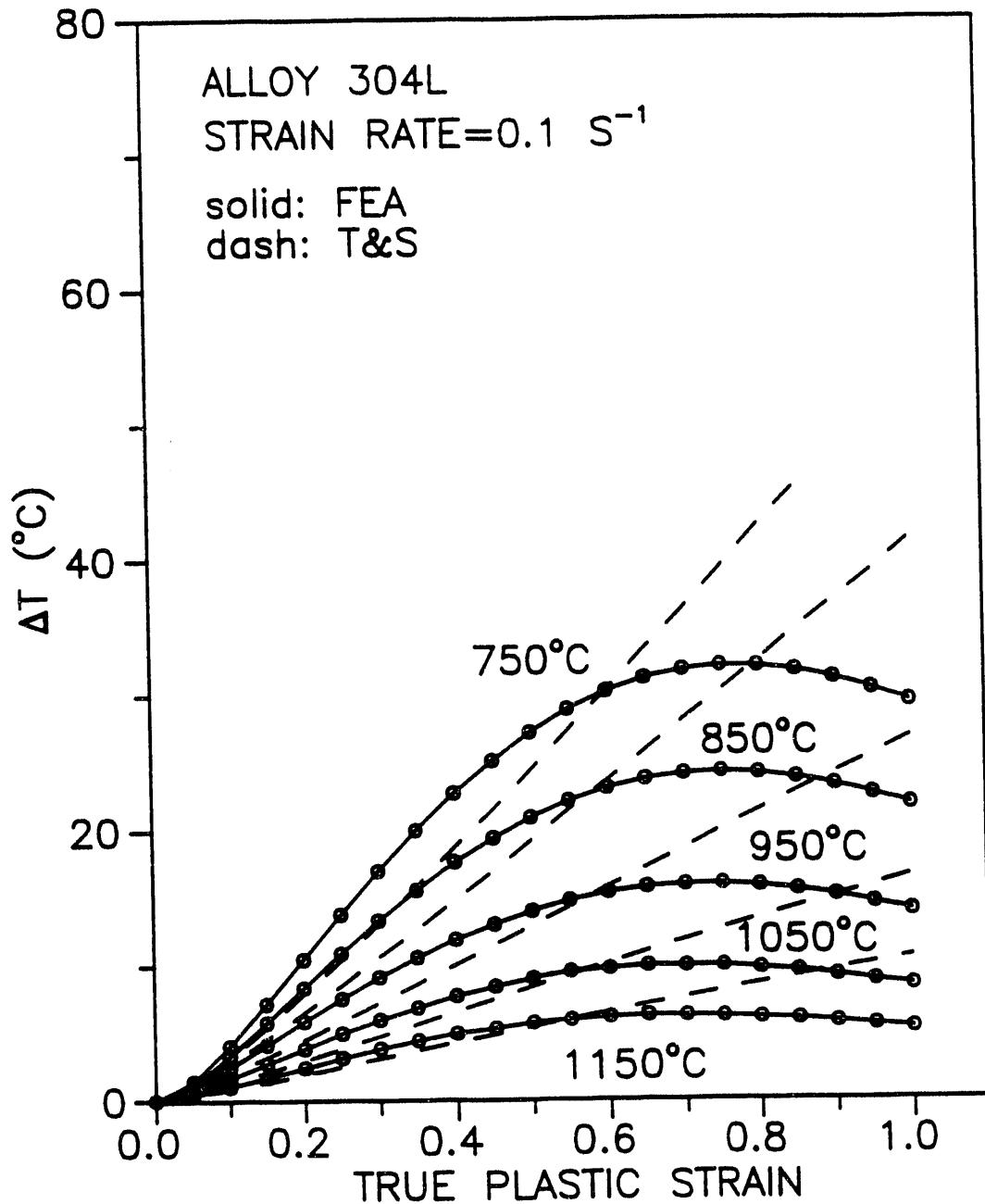


Figure 5. The change in specimen temperature with true plastic strain for alloy 304L compressed at a $\dot{\epsilon}$ of 0.1 s⁻¹. The initial test temperatures, between 750°C and 1150°C, are shown. Dashed curves were calculated by the method of Thomas and Shrinivasan¹³ and the solid curves are predicted by FEA.

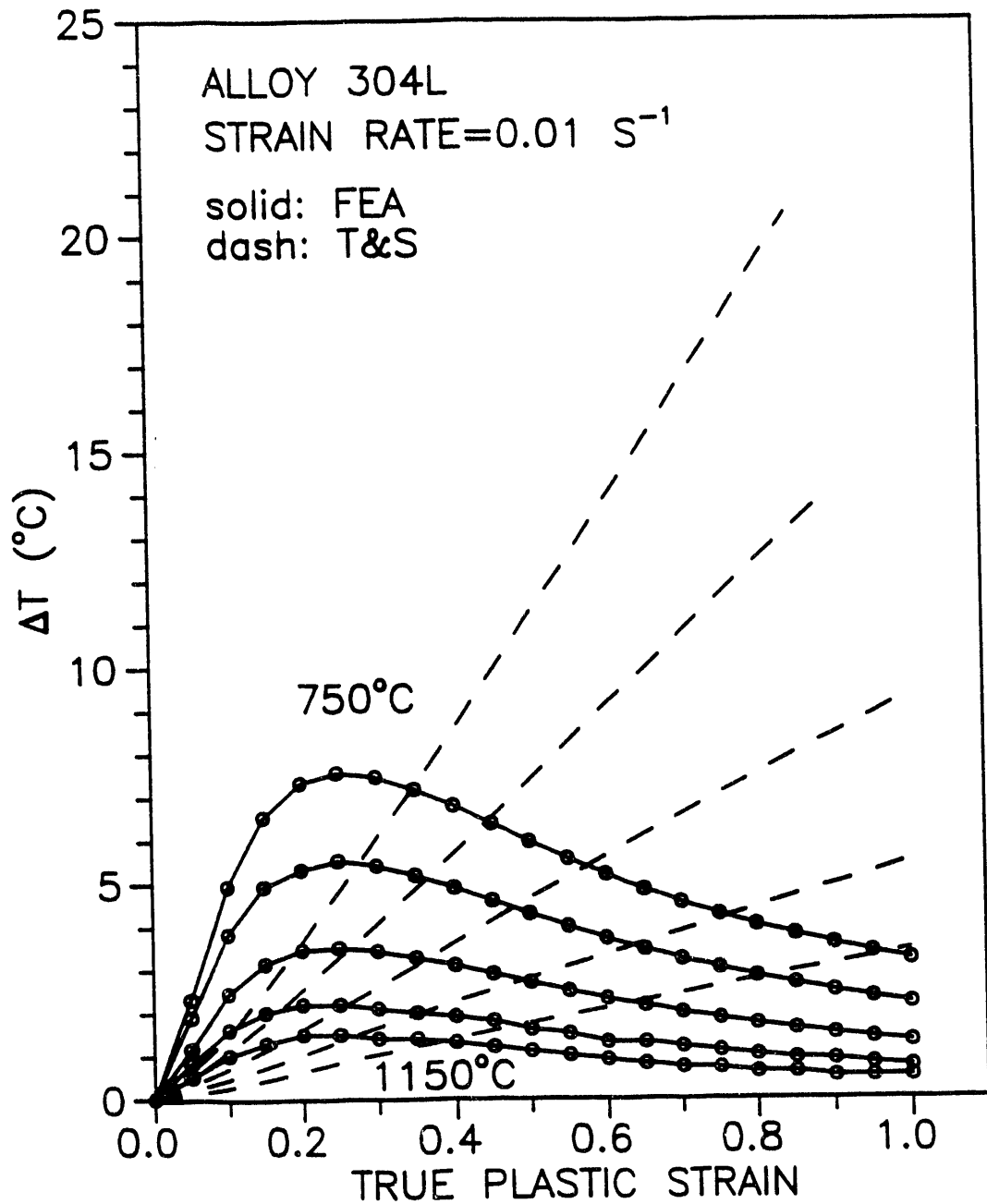


Figure 6. The change in specimen temperature with true plastic strain for alloy 304L compressed at a $\dot{\epsilon}$ of 0.01 s^{-1} . The initial test temperatures, between 750°C and 1150°C , are shown. Dashed curves were calculated by the method of Thomas and Shrinivasan¹³ and the solid curves are predicted by FEA.

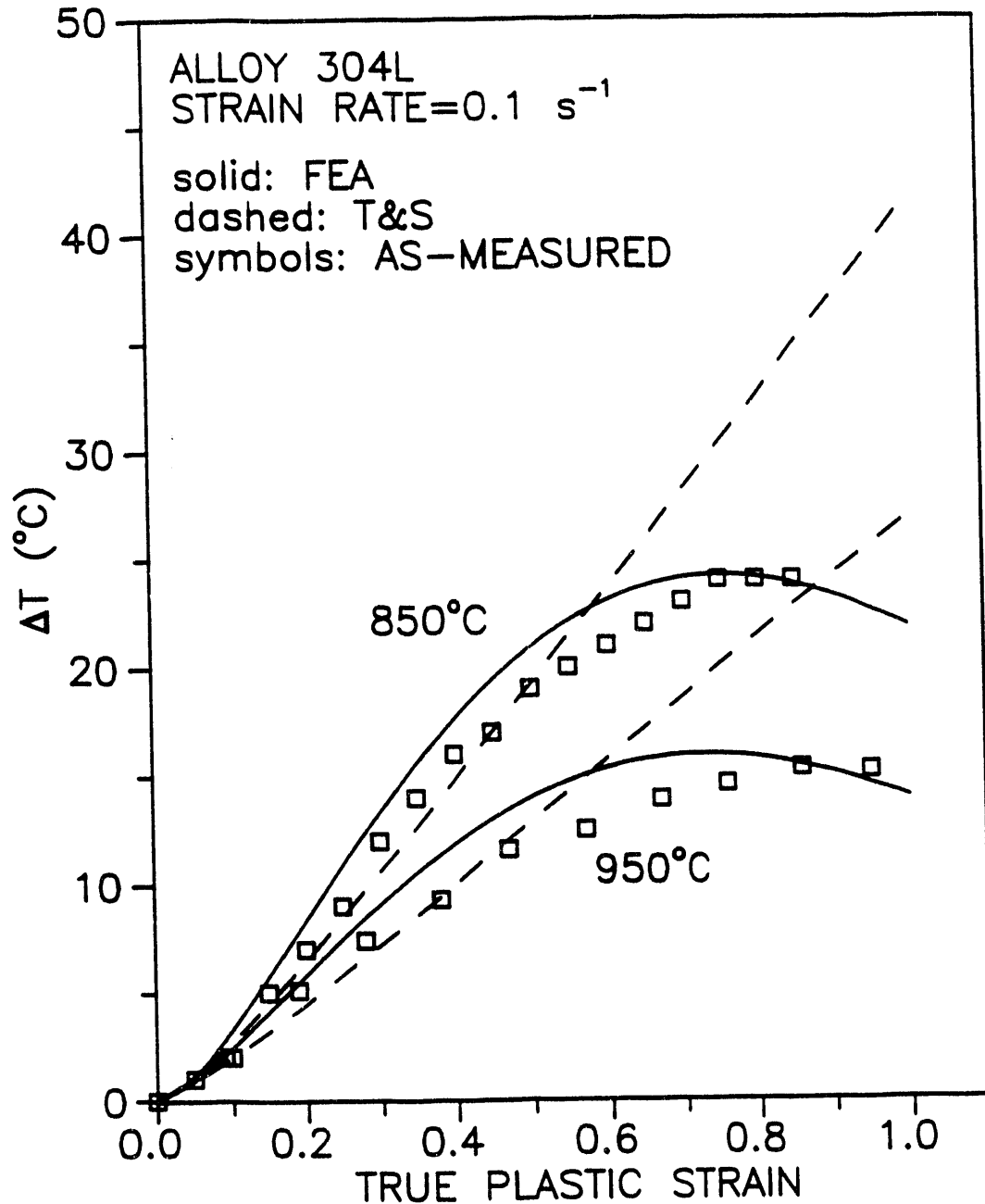


Figure 7. The change in specimen temperature with true plastic strain for alloy 304L compressed at a $\dot{\epsilon}$ of 0.1 s⁻¹, at temperatures of 850°C and 950°C. Dashed curves were calculated by the method of Thomas and Shrinivasan¹³. The solid curves are predicted by FEA. The open symbols (squares) were measured via an embedded thermocouple located at the center of the test specimen.

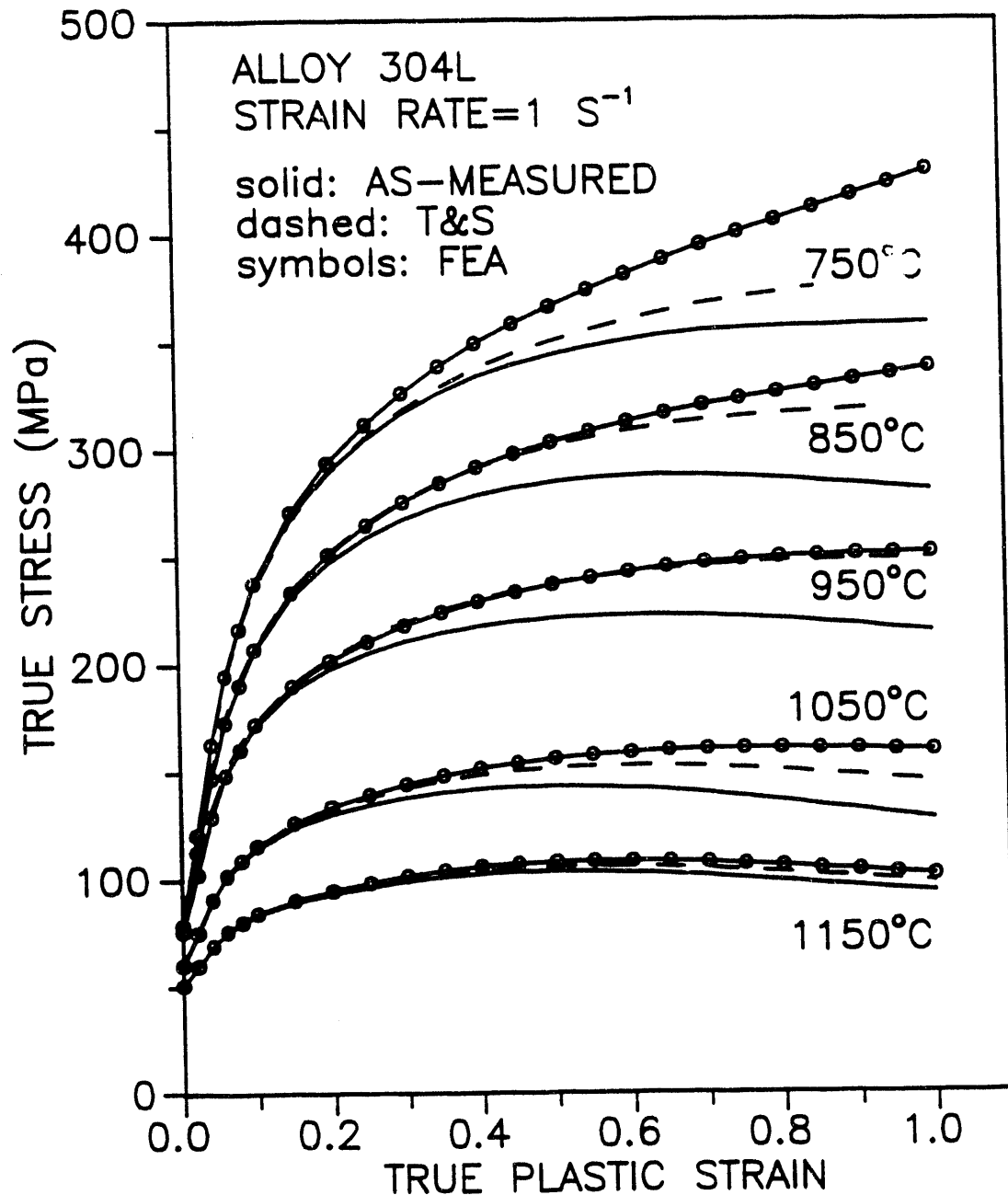


Figure 8. True stress versus true plastic strain for alloy 304L compressed at a $\dot{\epsilon}$ of 1 s^{-1} . The initial temperature of the tests ranged between 750°C and 1150°C . Solid curves are the as-measured behavior. Dashed curves are from the method of Thomas and Shrinivasan¹³. Solid curves with symbols (circles) are the isothermal curves from the FEA method.

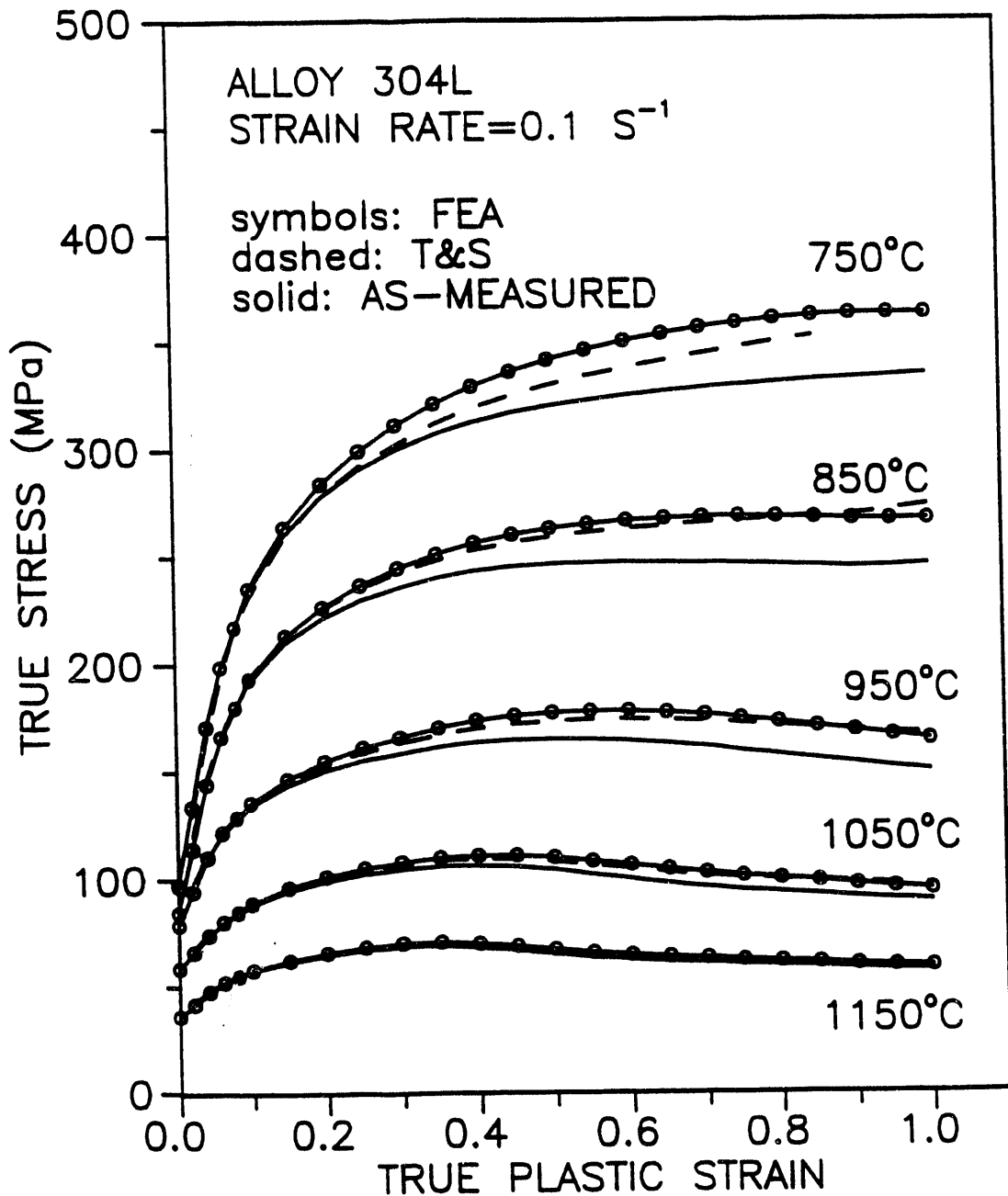


Figure 9. True stress versus true plastic strain for alloy 304L compressed at a $\dot{\epsilon}$ of 0.1 s⁻¹. The initial temperature of the tests ranged between 750°C and 1150°C. Solid curves are the as-measured behavior. Dashed curves are from the method of Thomas and Shrinivasan¹³. Solid curves with symbols (circles) are the isothermal curves from the FEA method.

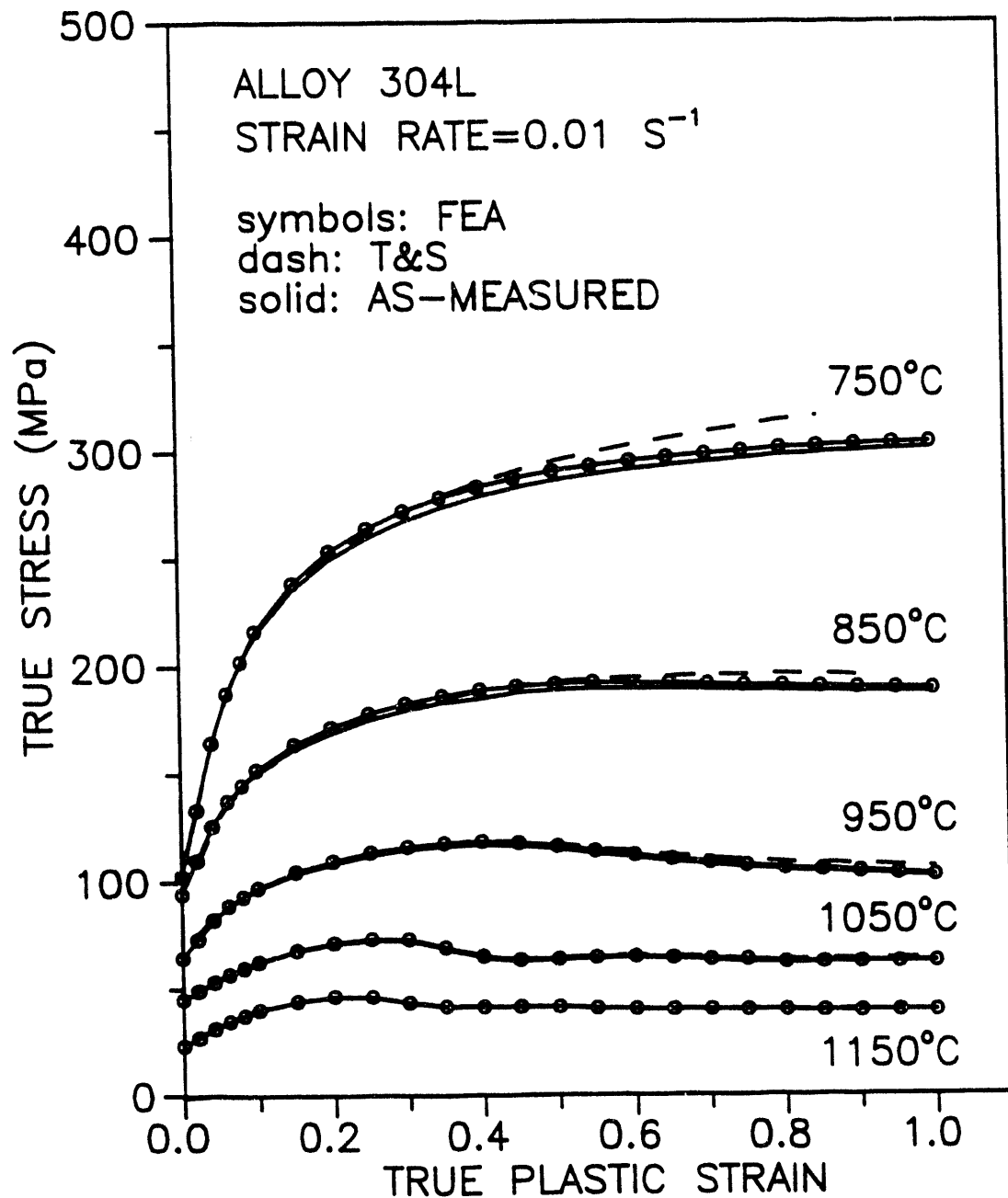


Figure 10. True stress versus true plastic strain for alloy 304L compressed at a $\dot{\epsilon}$ of 0.01 s⁻¹. The initial temperature of the tests ranged between 750°C and 1150°C. Solid curves are the as-measured behavior. Dashed curves are from the method of Thomas and Shrinivasan¹³. Solid curves with symbols (circles) are the isothermal curves from the FEA method.

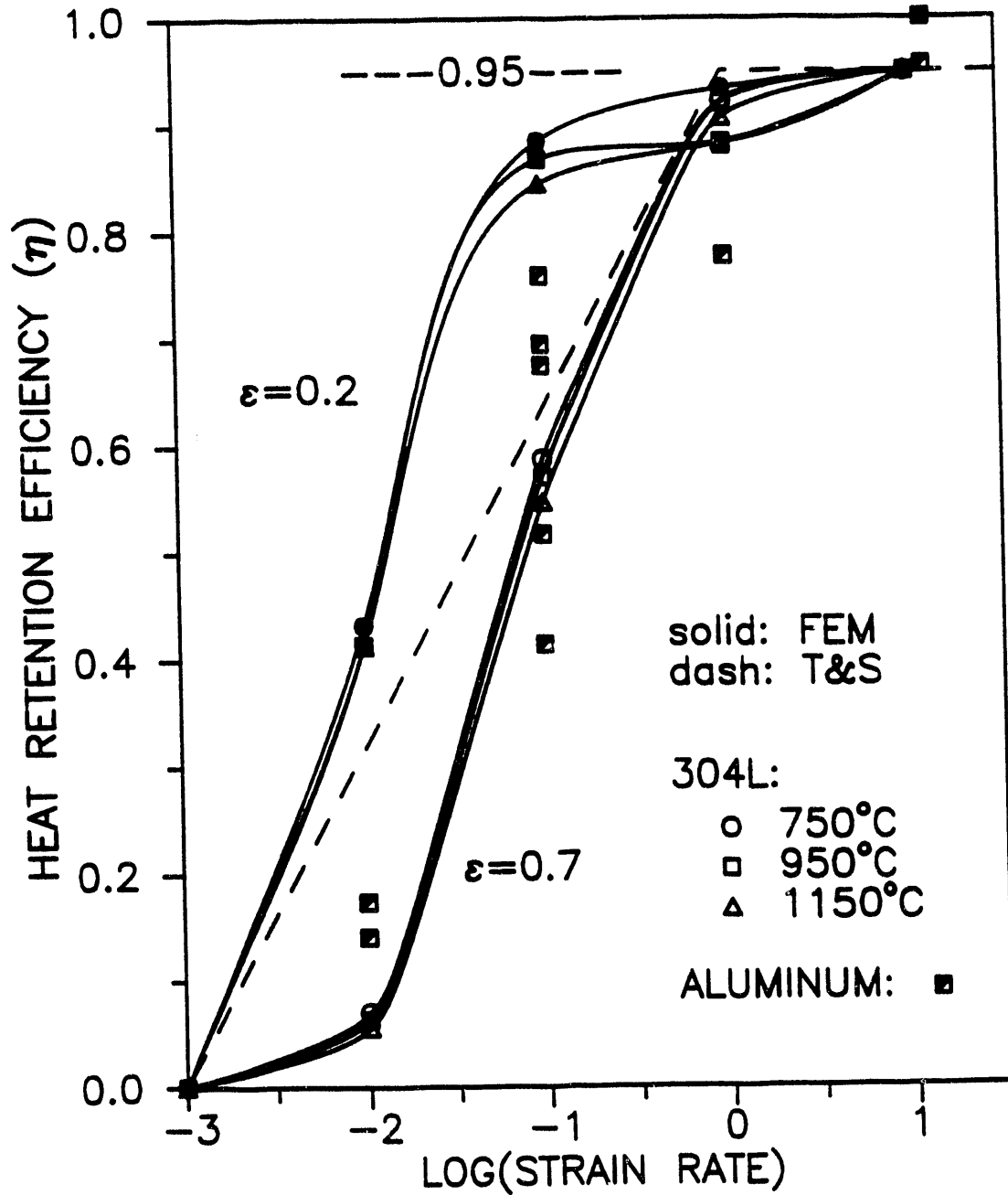


Figure 11. Heat retention efficiency, η , versus $\log \dot{\varepsilon}$ in the $\dot{\varepsilon}$ realm where conventional sized compression test samples of alloy 304L exhibit neither an isothermal nor an adiabatic state. η for both methods, FEA and Thomas & Shrinivasan are shown. Note the η from FEA is dependent while that from Thomas & Shrinivasan is independent of the applied strain. Data for aluminum is from Charpentier et al.¹⁴

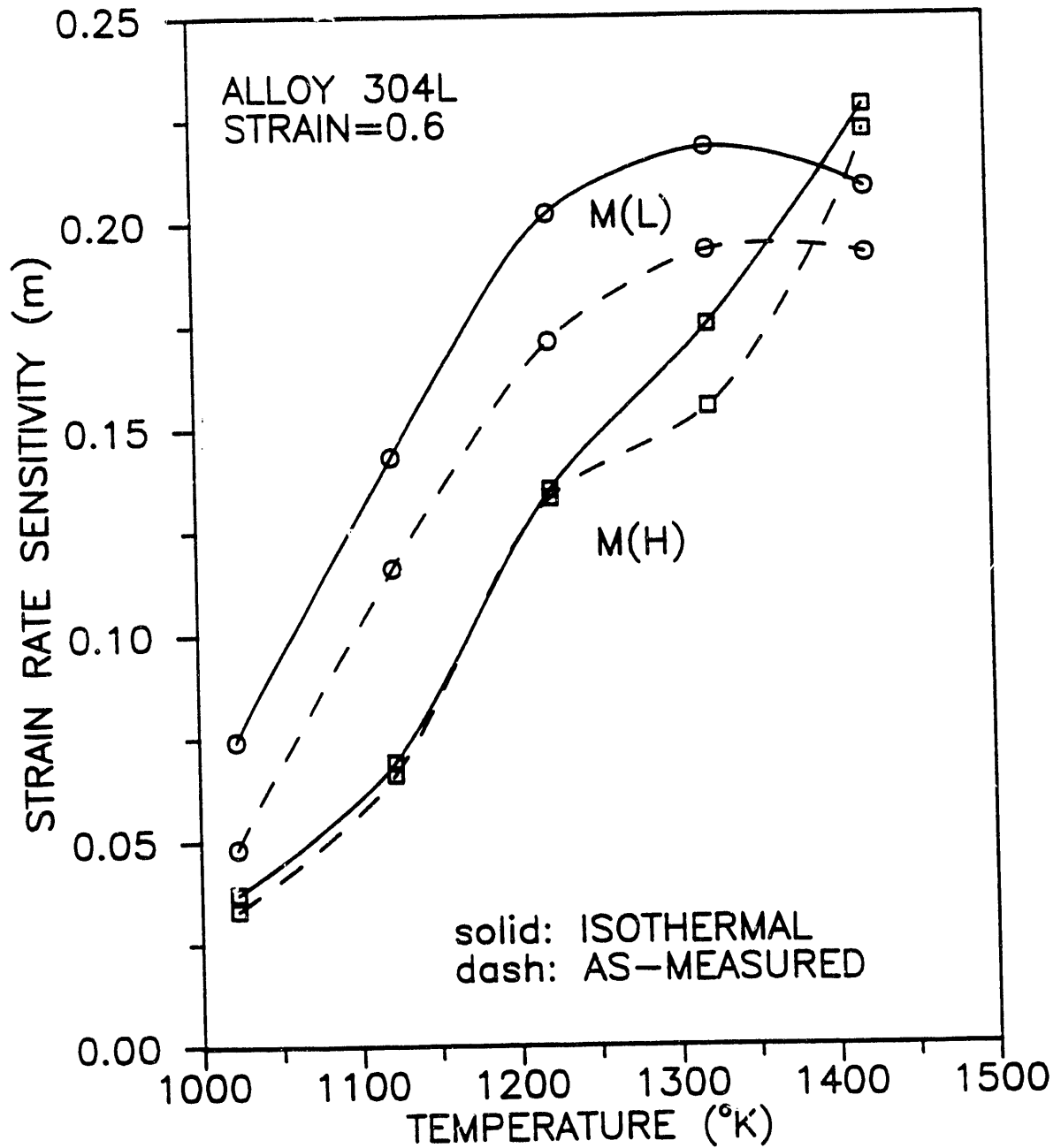


Figure 12. The variation of strain rate sensitivity, m , with the initial test temperature for alloy 304L compressed to a strain of 0.6. $M(L)$ is m calculated from the low $\dot{\epsilon}$ range, 0.01 s^{-1} to 0.1 s^{-1} ; $M(H)$ is from the high $\dot{\epsilon}$ range, 0.1 s^{-1} to 1 s^{-1} . Dashed curves were calculated from the as-measured stress-strain data while the solid curves are from the FEA isothermal data.

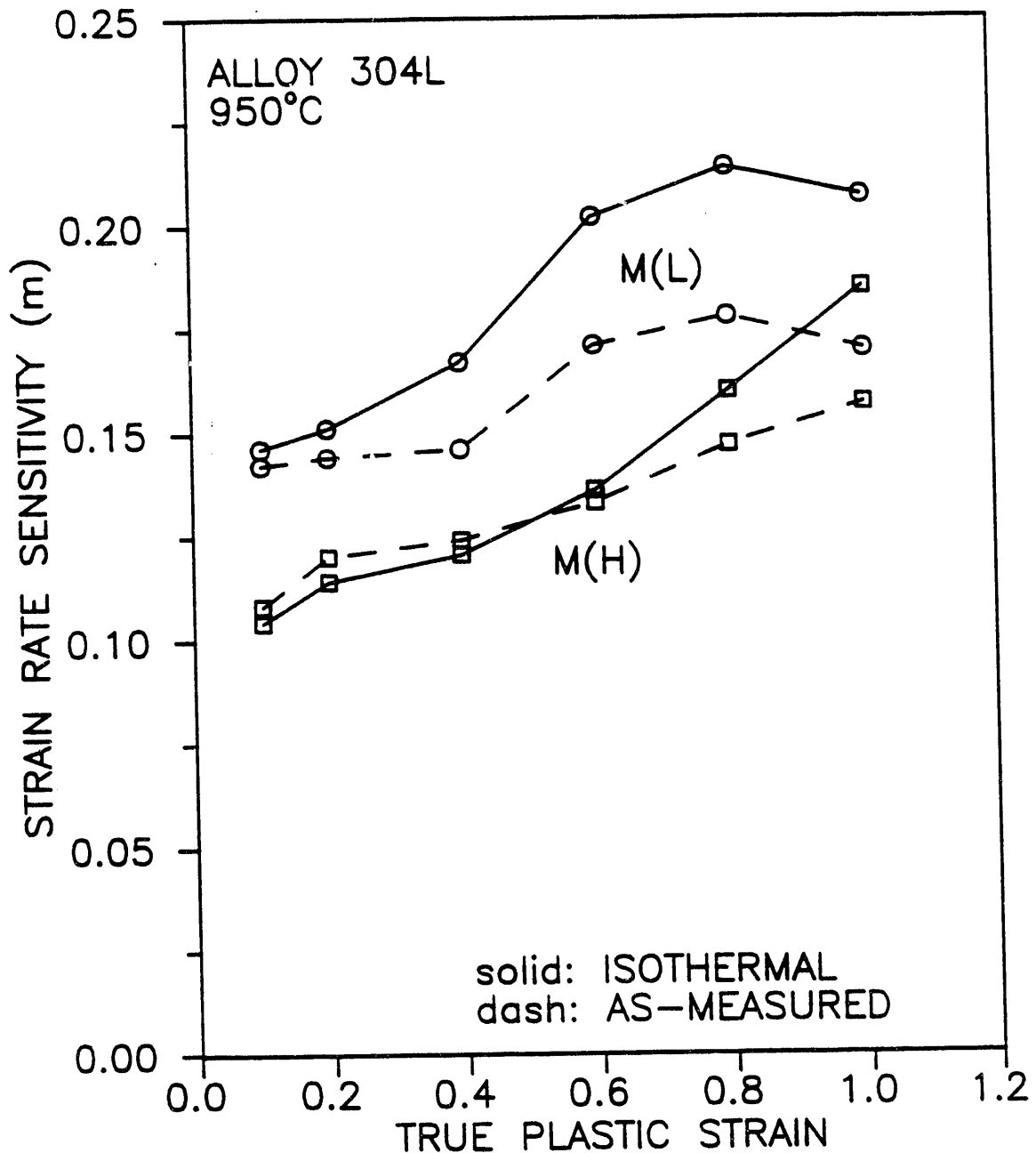


Figure 13. The variation of strain rate sensitivity, m , with true strain, for an initial test temperature of 950°C , for alloy 304L. $M(L)$ is m calculated for the low $\dot{\epsilon}$ range, 0.01 s^{-1} to 0.1 s^{-1} ; $M(H)$ is from the high $\dot{\epsilon}$ range, 0.1 s^{-1} to 1 s^{-1} . Dashed curves were calculated from the as-measured stress-strain data while the solid curves are from the FEA isothermal data.

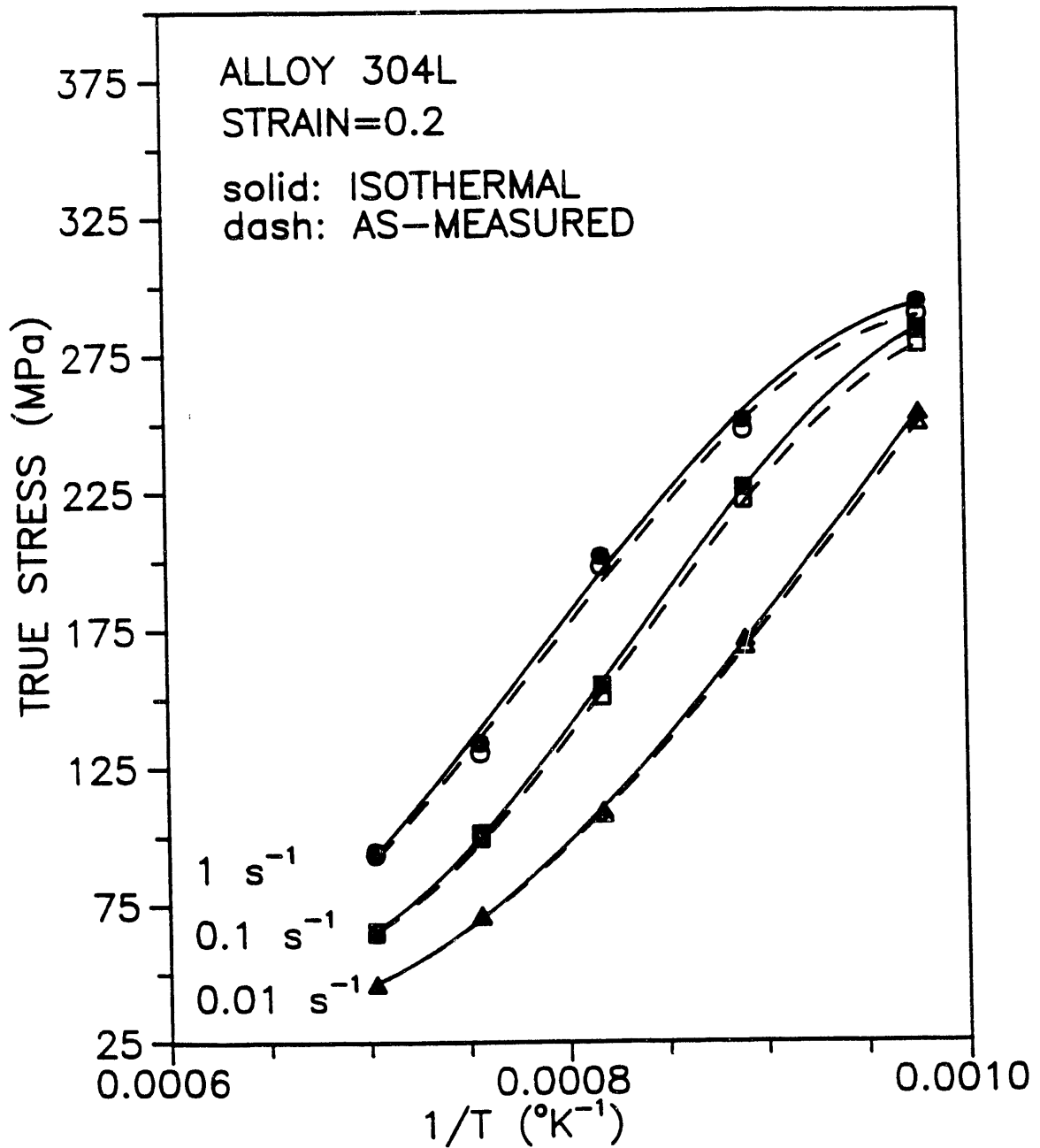


Figure 14. The variation of true stress with inverse temperature (kelvin⁻¹) for alloy 304L compressed at three different strain rates to a true strain of 0.2. Dashed curves are from the as-measured stress-strain data. The solid curves are from FEA isothermal data. Values of inverse temperature at various constant stress levels from this figure are utilized in Fig. 16.

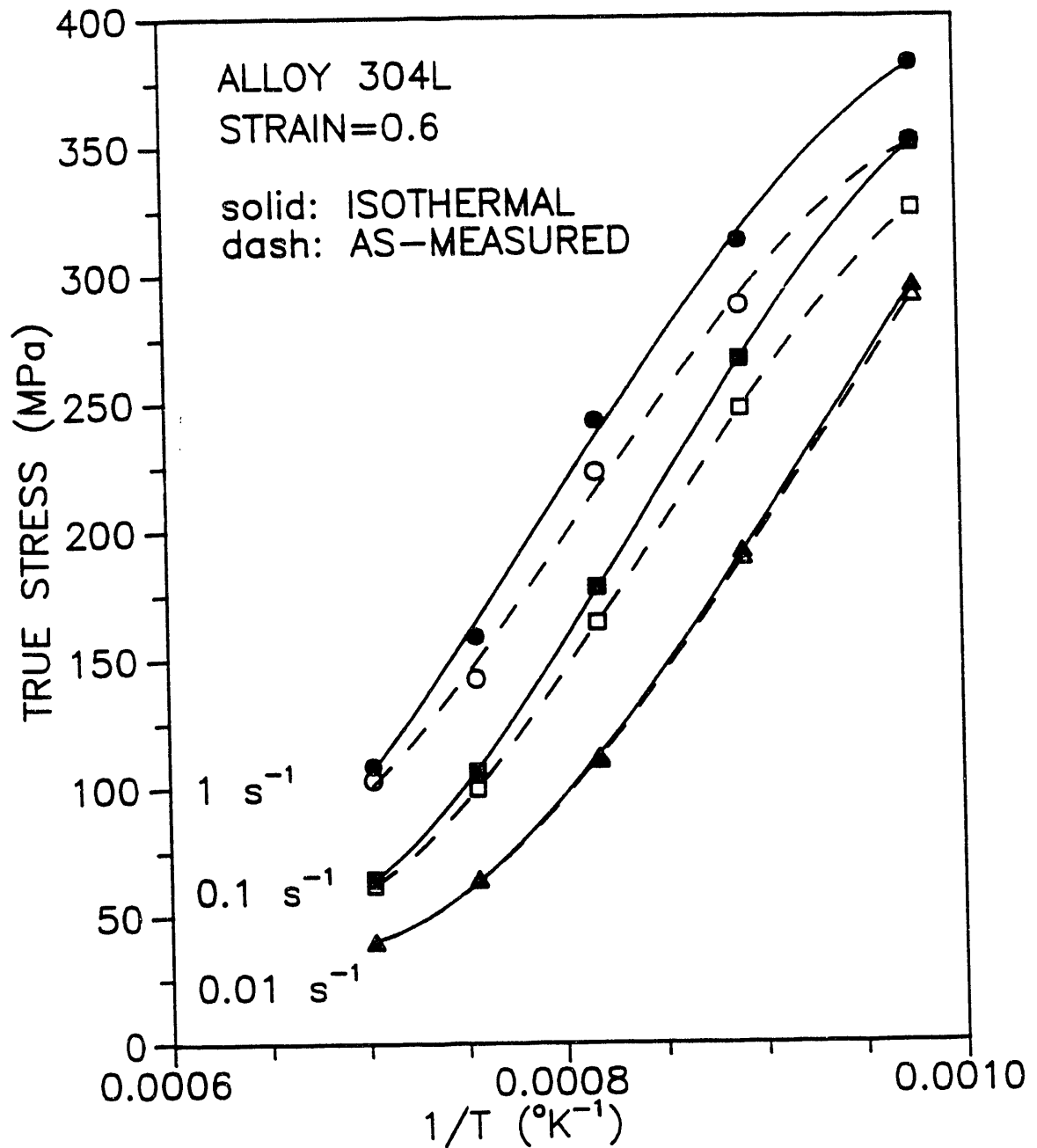


Figure 15. The variation of true stress with inverse temperature (kelvin⁻¹) for alloy 304L compressed at three different strain rates to a true strain of 0.6. Dashed curves are from the as-measured stress-strain data. The solid curves are from FEA isothermal data. Values of inverse temperature at various constant stress levels from this figure are utilized in Fig. 17.

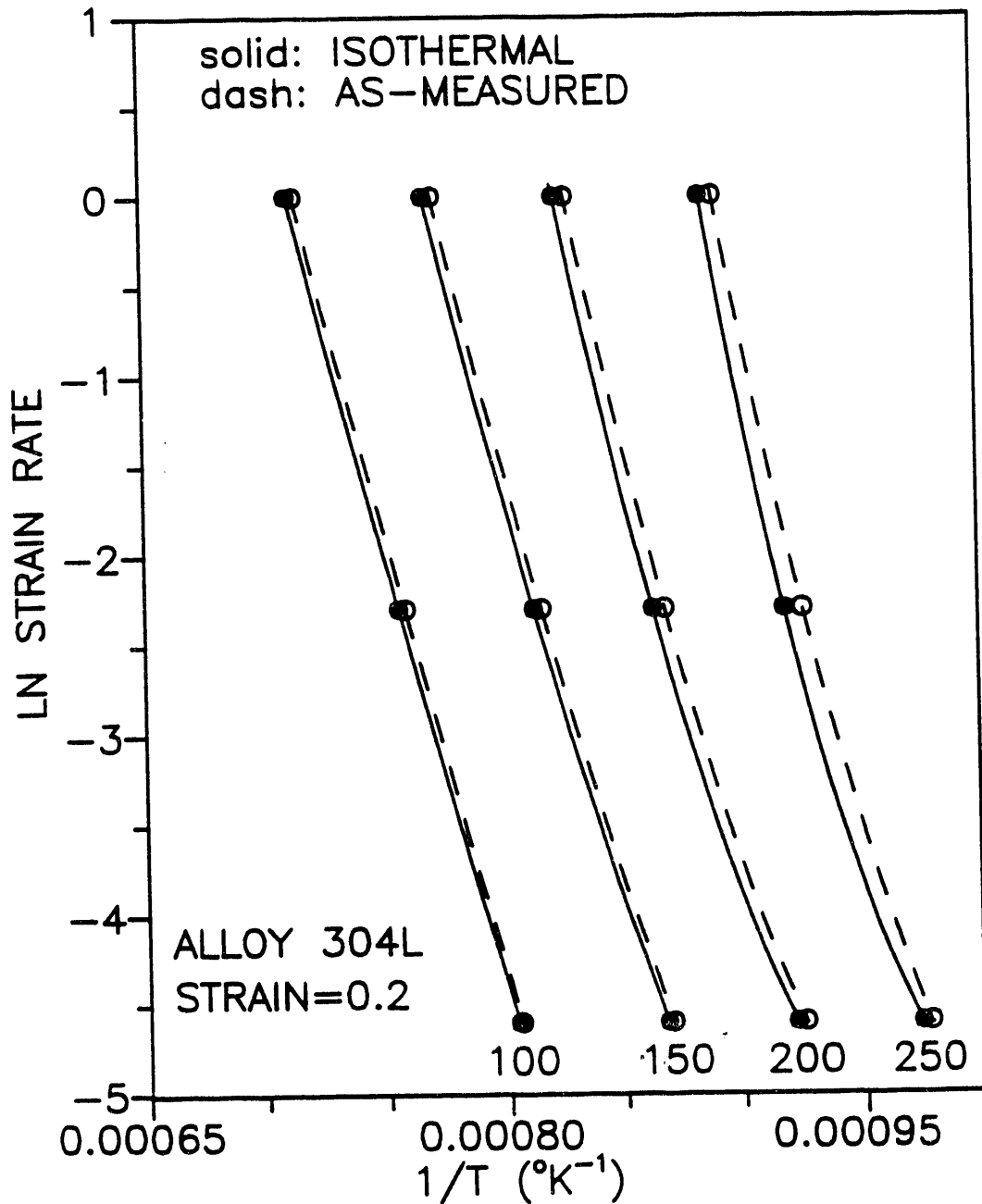


Figure 16. The variation in natural logarithm of strain rate with inverse temperature (kelvin⁻¹) at various constant stress levels, in MPa, for alloy 304L compressed to a strain of 0.2. Dashed curves are from the as-measured stress-strain data. The solid curves are from FEA isothermal data.

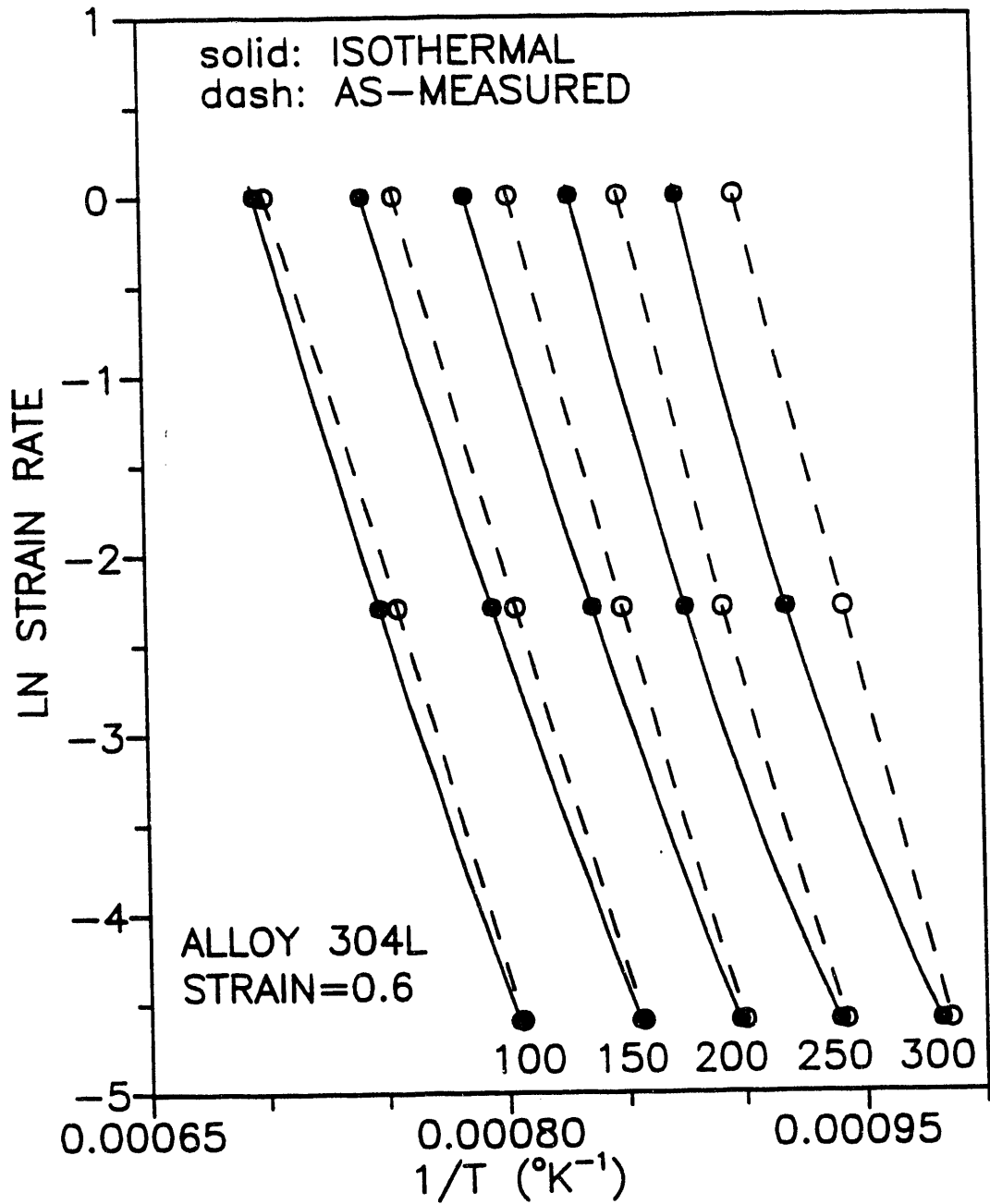


Figure 17. The variation in natural logarithm of strain rate with inverse temperature (kelvin^{-1}) at various constant stress levels, in MPa, for alloy 304L compressed to a strain of 0.6. Dashed curves are from the as-measured stress-strain data. The solid curves are from FEA isothermal data.

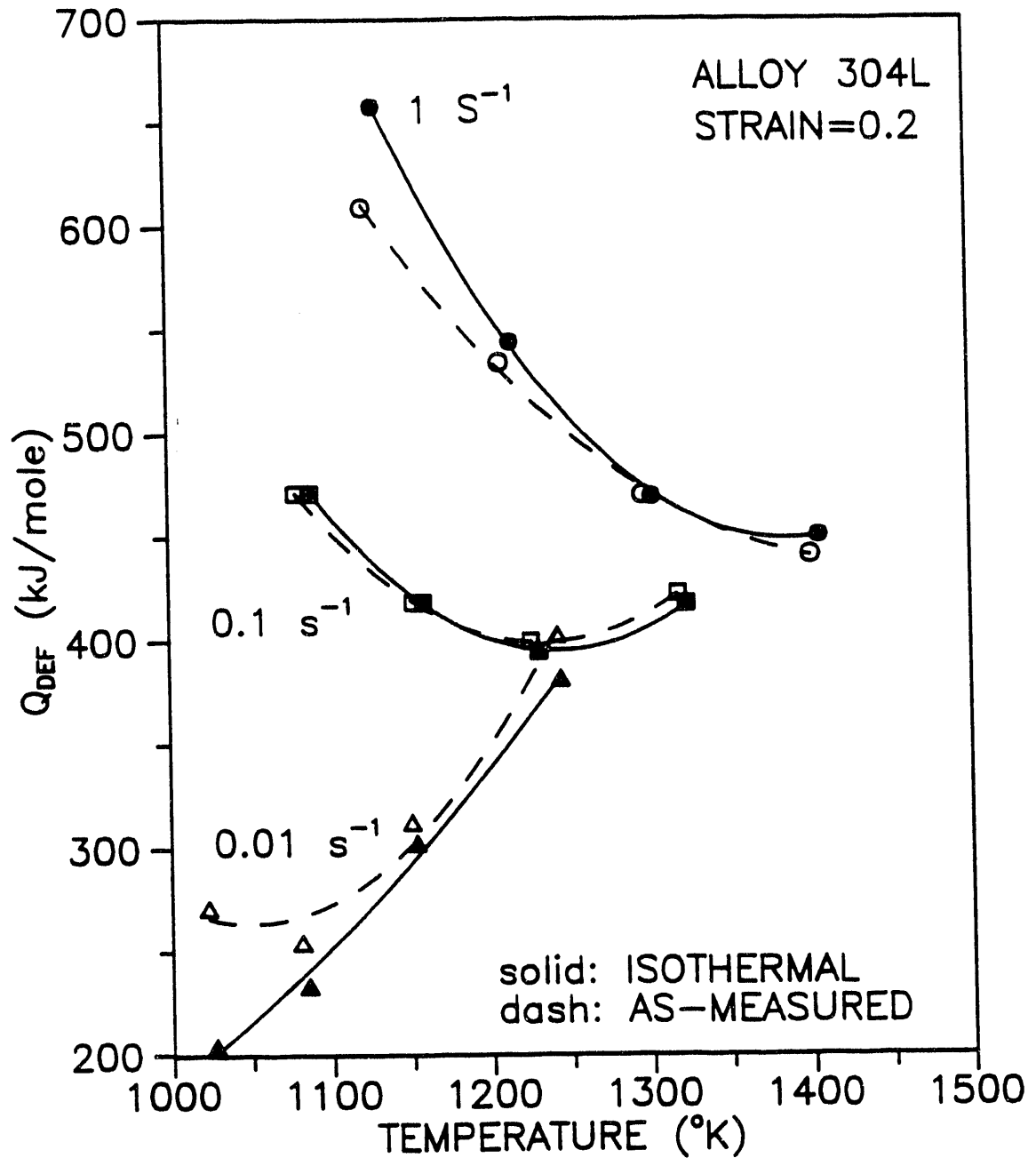


Figure 18. The variation of activation energy, Q_{DEF} , with initial deformation temperature for alloy 304L compressed at three different strain rates to strain of 0.2. Dashed curves are from the as-measured stress-strain data. The solid curves are from FEA isothermal data.

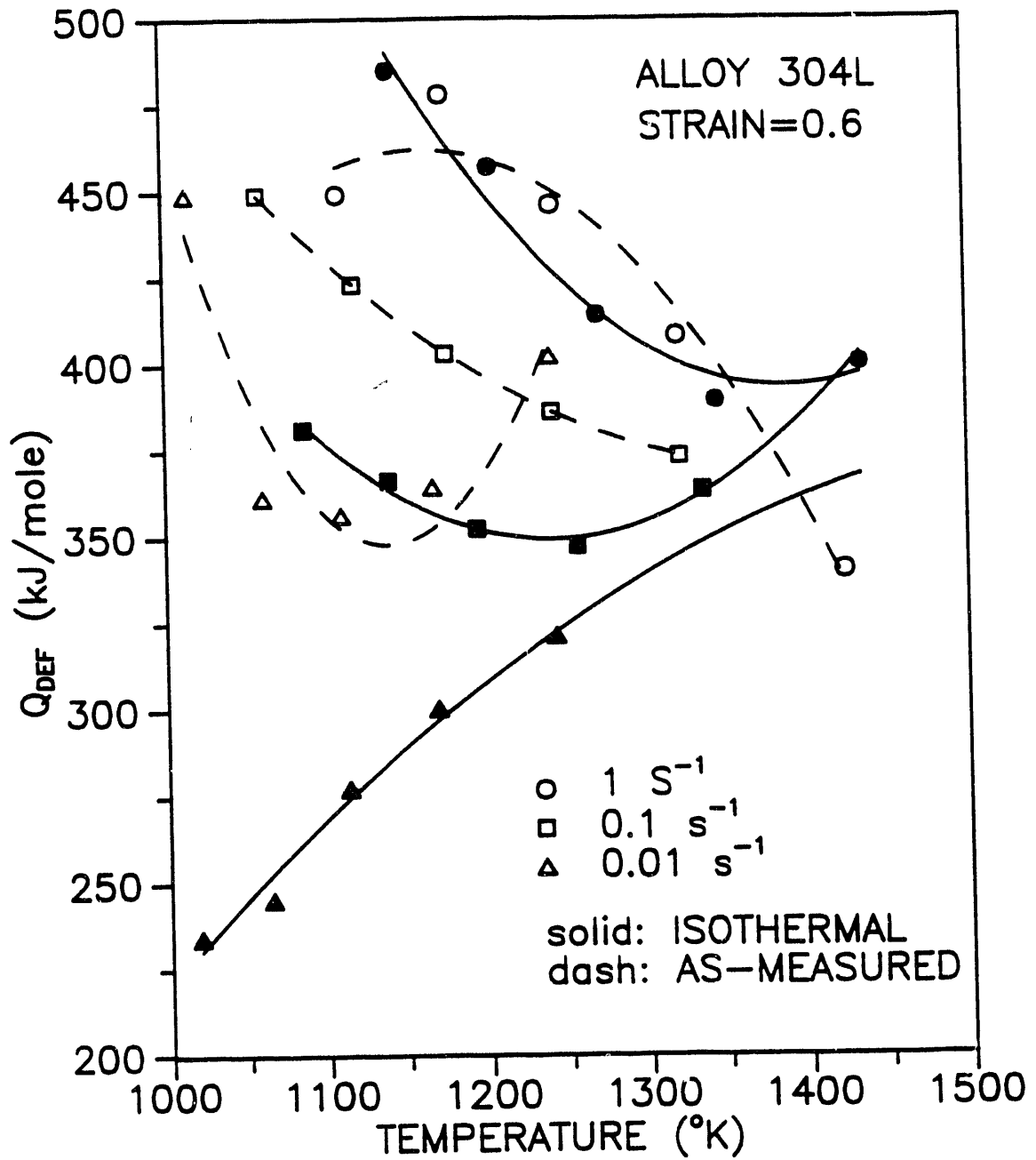


Figure 19. The variation of activation energy, Q_{DEF} , with initial deformation temperature for alloy 304L compressed at three different strain rates to strain of 0.6. Dashed curves are from the as-measured stress-strain data. The solid curves are from FEA isothermal data.

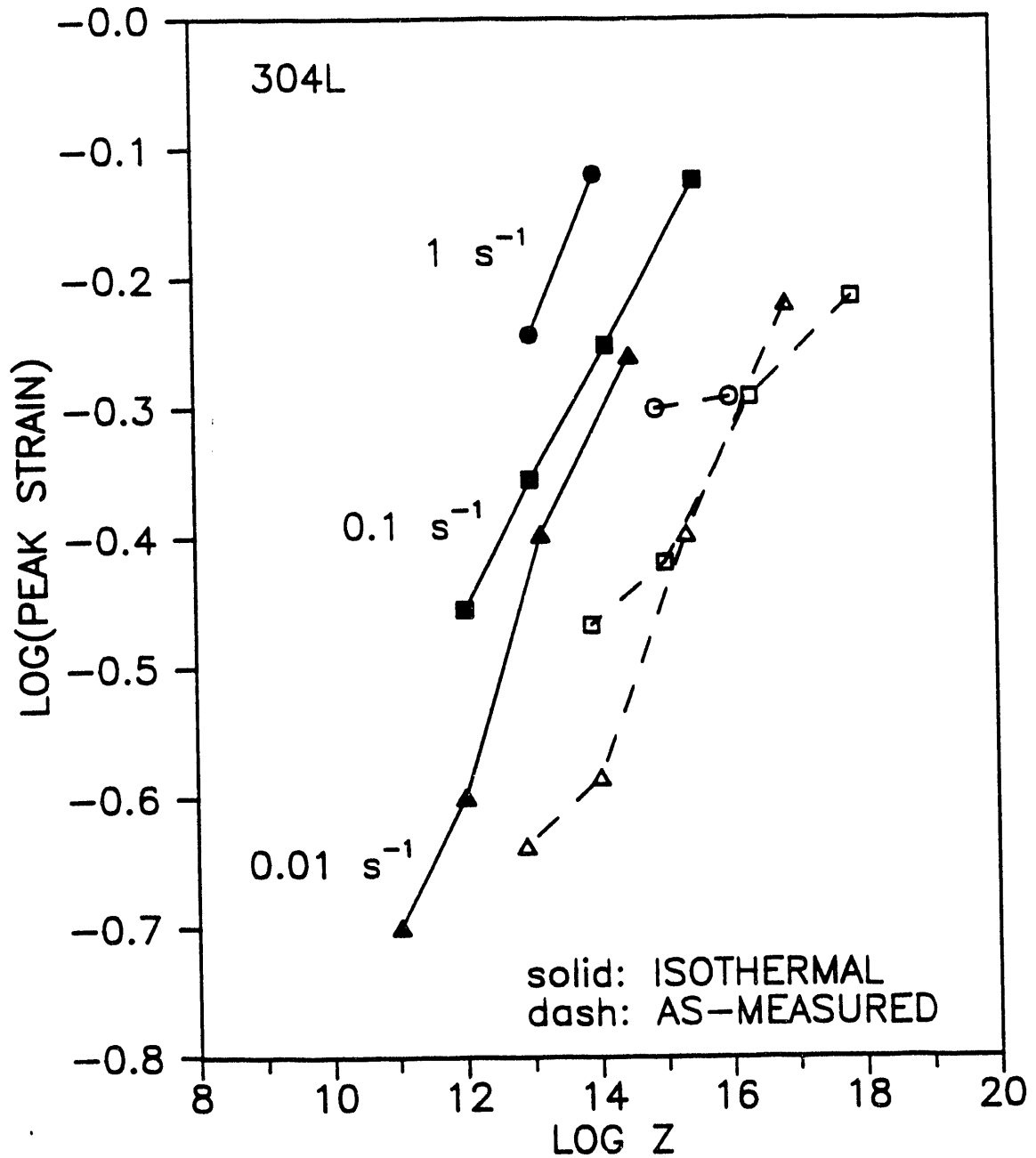


Figure 20. Variation of logarithm peak strain with logarithm Z for 304L deformed at three different strain rates. Dashed curves originate from as-measured stress-strain data and Q_{DEF} in Z is assumed to have a constant value of 407 kJ/mole from Table VI. The solid curves are from FEA isothermal data and Q_{DEF} has a value of 356 kJ/mole from Table VI.

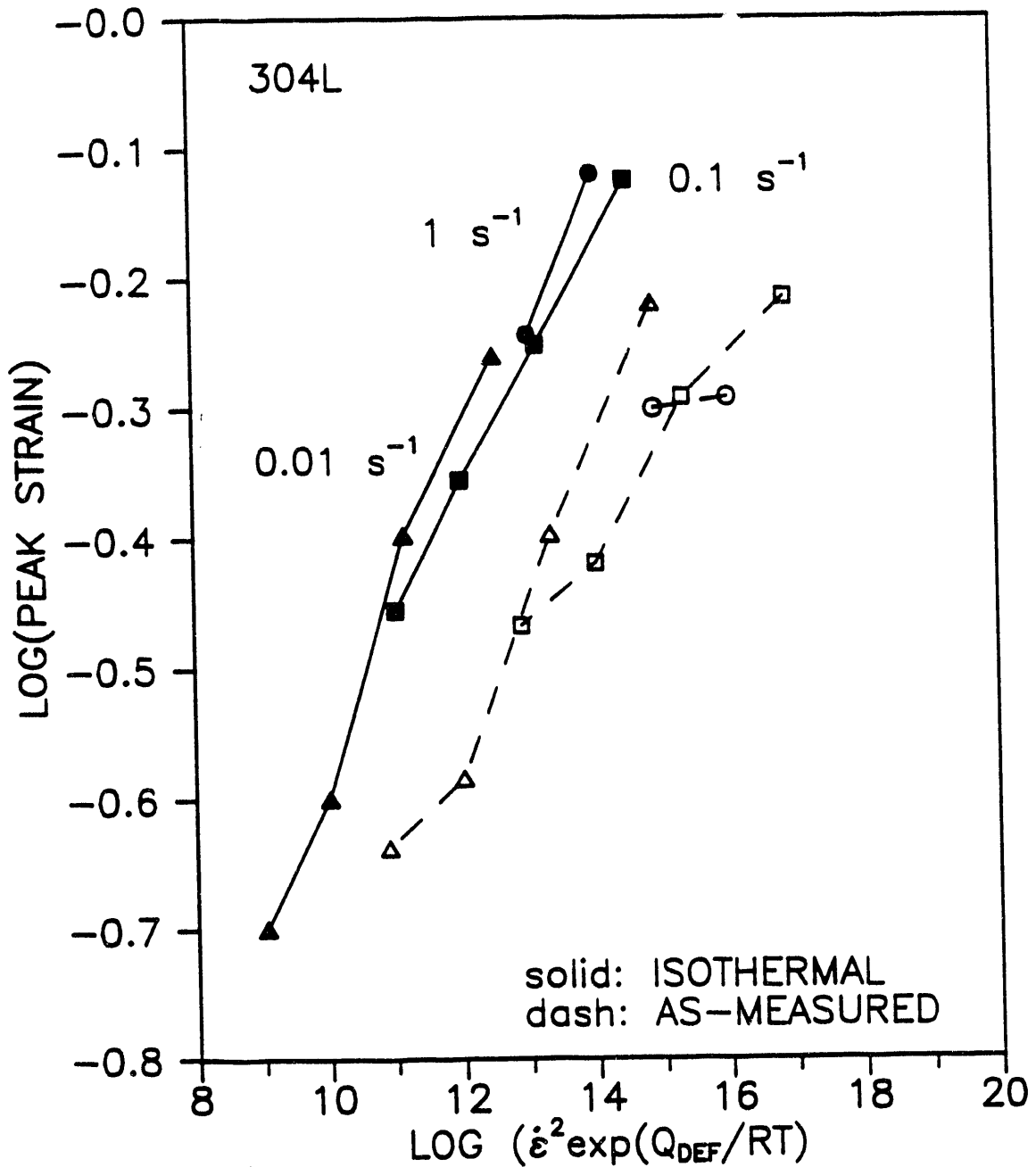


Figure 21. Variation of logarithm peak strain with logarithm Z_{modified} , where the power on strain rate in Z is 2 rather than 1, for 304L deformed at three different strain rates. Dashed curves originate from as-measured stress-strain data and Q_{DEF} in Z is assumed to have a constant value of 406 kJ/mole from Table VI. The solid curves are from FEA isothermal data and Q_{DEF} has a value of 355 kJ/mole from Table VI. Logarithm of peak strain versus logarithm of a modified Z .

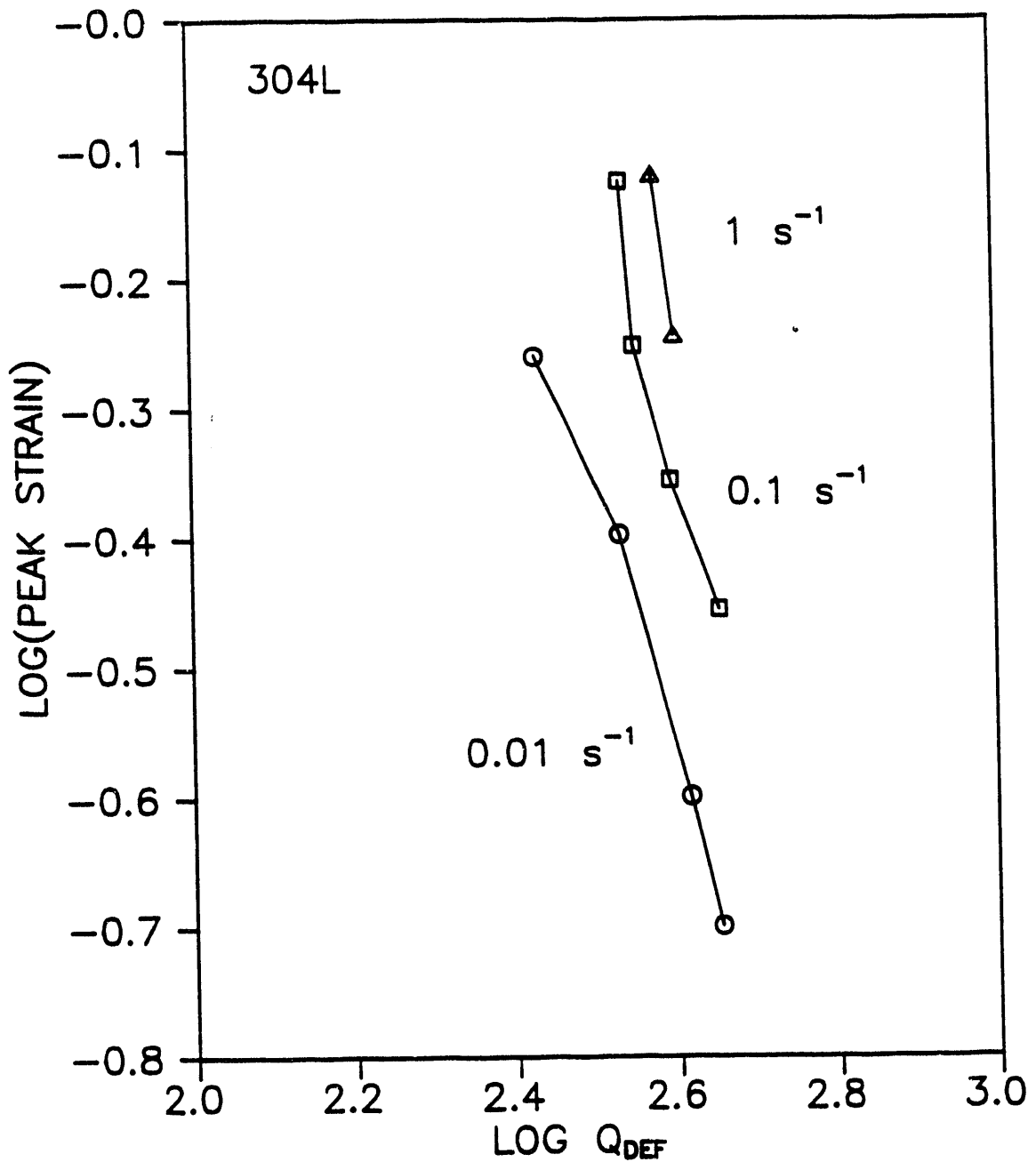


Figure 22. Variation of logarithm peak strain with logarithm Q_{DEF} for 304L compressed at three different strain rates. Values for Q_{DEF} assumed to vary with strain rate and temperature, are listed in Table VI.

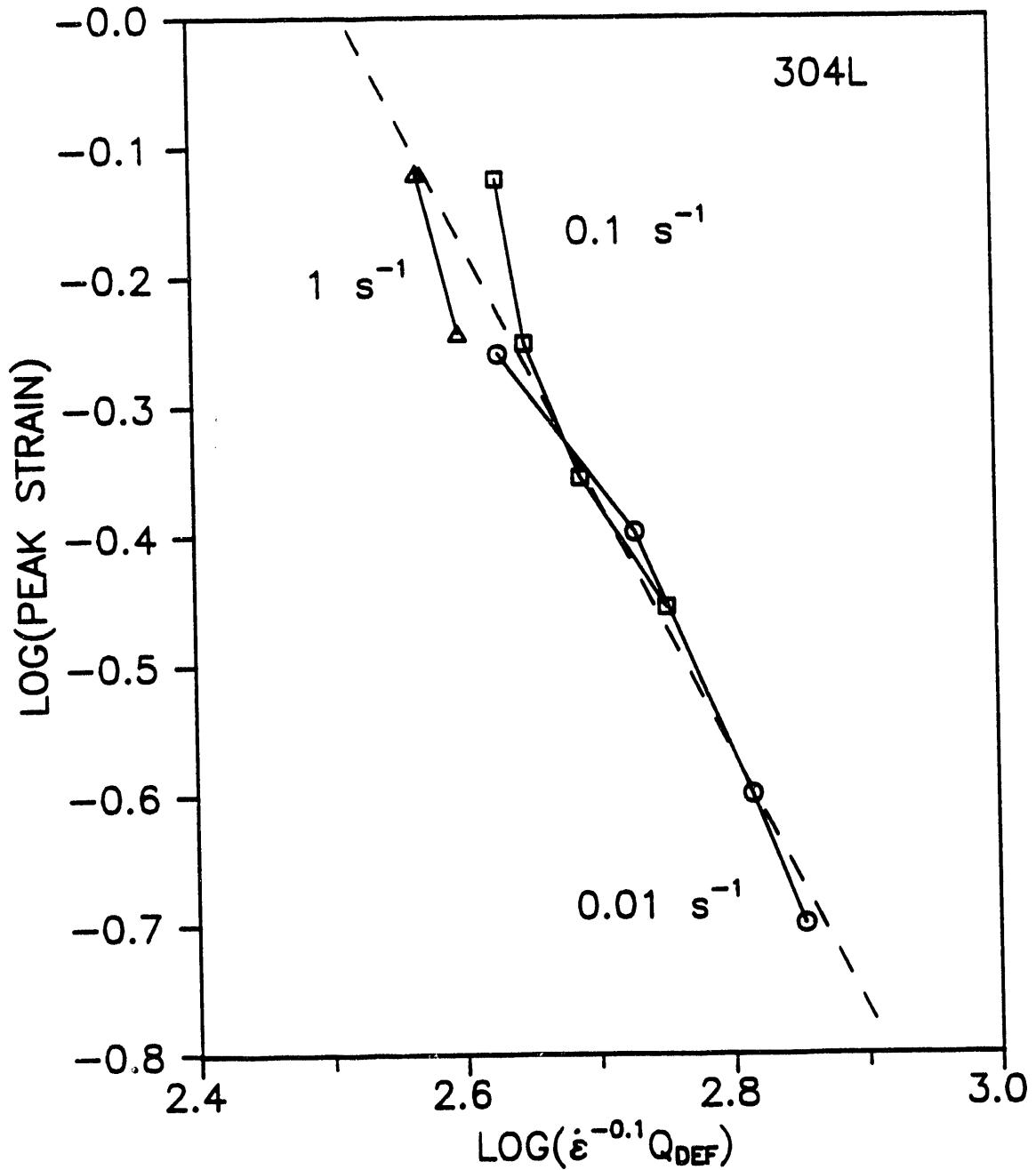


Figure 23. Variation of logarithm peak strain with logarithm ($\dot{\epsilon}^{-0.1} Q_{DEF}$) for 304L compressed at three different strain rates. Values for Q_{DEF} assumed to vary with strain rate and temperature, are listed in Table VI. Inclusion of the strain rate term, $\dot{\epsilon}^{-0.1}$, unifies the relationship, shown in Fig. 22. The unifying equation is $\epsilon_p = A\dot{\epsilon}^{0.2}/Q^2$, where $A = 1.015 \times 10^5$ mole sec/kJ.

END

**DATE
FILMED**

9/29/93

